## Chapter B

# Conditions of Metamorphism in Lower-Plate Rocks at Bare Mountain, Nevada—Implications for Extensional Faulting

*By* Thomas D. Hoisch[1]

## Contents

Abstract ..... 2
Introduction ..... 2
Acknowledgments ..... 4
General Geology of Bare Mountain ..... 4
Higher Grade Rocks of the Metamorphosed Block ..... 4
    Mica Schists ..... 4
        Mineral Reactions and Isograds ..... 4
        Garnet Growth Simulations ..... 8
        Garnet-in, Chlorite-out Simulation ..... 8
    Thermodynamic Data ..... 9
        Thermobarometry ..... 9
    Siliceous Metadolomite ..... 13
        Mineral Reactions ..... 13
        Calcite-Dolomite Geothermometry ..... 15
Lower Grade Rocks of the Metamorphosed Block ..... 16
North-Central, Northeastern, and Eastern Bare Mountain ..... 16
Significance of the Metamorphism ..... 17
Timing of Detachment Faulting ..... 21
Conclusions ..... 22
References Cited ..... 22

## Figures

1. Simplified geologic map of Bare Mountain and surrounding areas ..... 3
2. Simplified geologic map of northwestern Bare Mountain ..... 5
3. Stability diagram of coexisting quartz + muscovite + chlorite + biotite + staurolite + garnet as a function of garnet composition ..... 8
4. Diagrams showing garnet zoning profiles and model growth simulations ..... 12
5. Diagram showing calculated isopleths of garnet absent and chlorite absent for garnet from sample from northwestern Bare Mountain ..... 15
6. Diagrams showing thermobarometry based on mineral compositions in garnet schists from northwestern Bare Mountain ..... 19
7. Diagram showing selected reactions in the system $MgO$-$CaO$-$SiO_2$-$CO_2$-$H_2O$ at 5 kilobars ..... 20
8. Bar diagram showing calcite-dolomite geothermometry from a sample from northwestern Bare Mountain ..... 21

[1]Northern Arizona University, Flagstaff, Ariz.

# Tables

1. Mineral assemblages in mica schists and metacarbonate rocks from northwestern Bare Mountain ..... 6
2. Chemical composition of garnet cores and rims, micas, plagioclase, and chlorite from northwestern Bare Mountain ..... 9
3. Mineral analyses and specified values for simulations of growth in garnets from northwestern Bare Mountain ..... 17
4. Minerals, modes, and activity assumptions for the calculation of garnet-in and chlorite-out isopleths in figure 5 ..... 18
5. Changes in mode and composition between garnet-in and chlorite-out isopleths at 5 kilobars ..... 18
6. Garnet-biotite and garnet-chlorite geothermometric determinations in rocks from northwestern Bare Mountain ..... 18

[For table of abbreviations and conversions, click here]

## Abstract

Metamorphosed supracrustal rocks are exposed beneath a Tertiary detachment (low-angle normal) fault in several mountain ranges west of Yucca Mountain, Nevada. The closest exposure to Yucca Mountain is at Bare Mountain, 20 kilometers to the west. The extent and timing of lower-plate unroofing are important to understanding the evolution of the detachment fault. In this investigation, petrologic methods were applied to the metamorphic rocks at Bare Mountain to determine the extent of unroofing since the peak of metamorphism in Early Cretaceous time.

Bare Mountain is flanked on the north by a north-dipping detachment fault, the Fluorspar Canyon fault, which juxtaposes Tertiary volcanic rocks in the upper plate against a thick sequence of variably metamorphosed Paleozoic sedimentary rocks in the lower plate. The metamorphic rocks are confined to a block in the northwestern part of the lower plate that is bounded on the north by the Fluorspar Canyon fault and on the east by an east-dipping normal fault, the Gold Ace fault. The northern part of the block is metamorphosed to lower amphibolite facies, where mica schists of the Wood Canyon Formation contain the mineral assemblage quartz+chlorite+muscovite+biotite+plagioclase±garnet±staurolite. Lower amphibolite facies conditions are consistent with reactions that limit the stability of coexisting garnet+chlorite+staurolite+biotite in mica schist, with the preservation of growth zoning in garnets, with mineral assemblages observed in siliceous metadolomites, and with calcite-dolomite geothermometry. Thermobarometry based on quartz+plagioclase+garnet+biotite+muscovite equilibria indicates conditions of 530°±50°C and 5.3±1.5 kilobars (18.6±5.3 kilometer-depth). The thermobarometry calculations incorporate a correction to the biotite composition that was needed to compensate for iron enrichment that took place during retrograde metasomatism.

Within the fault-bounded block, metamorphic grade and grain size decrease to the southeast, which implies a postmetamorphism tilt to the southeast. About 3 kilometers south of the northwest corner of the lower plate, an isograd delineates the southern limit of garnet and staurolite in the Wood Canyon Formation. A metamorphic grade discordance occurs across the Gold Ace fault. Conodont color-alteration indexes indicate that conditions of middle greenschist to subgreenschist facies were attained in the hanging wall, which is consistent with locally observed fossils in shales.

Thermochronologic data indicate that the final ≈9 kilometers of unroofing of the northwestern part of Bare Mountain took place rapidly (rapid cooling) from 12.6 to 11.1 million years ago as a result of tectonic denudation by detachment faulting. This was preceded by ≈9 kilometers of slow unroofing (slow cooling) probably related to surface erosion. Models of detachment faulting must take into consideration ≈9 kilometers of unroofing of the northwestern part of Bare Mountain and a large component of normal displacement (≈4 kilometers) across the Gold Ace fault.

## Introduction

The Death Valley region of southwest Nevada and adjacent California is characterized by major Tertiary and Quaternary crustal extension (Applegate and others, 1992; Hamilton 1988a, 1988b; Hodges and Walker, 1990; Hoisch and Simpson, 1993; Holm and Dokka, 1991, 1993; Holm and others, 1992, 1993; Holm and Wernicke, 1990). Crustal extension was accommodated by high-angle normal faults and larger regional detachment (low-angle normal) faults; many normal faults sole into or are truncated at their bases by the larger regional detachments. Deep-seated metamorphosed supracrustal rocks are exposed in the lower plates of detachment faults in several mountain ranges.

A regional detachment fault can be traced through three mountain ranges west of Yucca Mountain. From east to west, the named fault segments are: the Fluorspar Canyon fault along the northern margin of Bare Mountain, the Bullfrog detachment fault in the southern Bullfrog Hills, and the Boundary Canyon fault in the Funeral Mountains (fig. 1). The three fault segments were initially correlated by Carr and Monsen (1988). Metamorphosed supracrustal rocks are exposed in the lower plate. Geophysical data suggest that the lower plate is continuous from Bare Mountain across the Amargosa Desert, where it is unexposed, to the Funeral Mountains. Gravity (A.E. McCafferty and V.J.S. Grauch, written commun., 1994) and magnetic (Glen and Ponce, 1991) data for the Amargosa Desert, which separates Bare Mountain from the Funeral Mountains (fig. 1), suggest a shallow basin fill and no major structures.

This study applied petrologic methods to metamorphic rocks in the lower plate of the Fluorspar Canyon fault at Bare Mountain, 20 km west of Yucca Mountain. Eighty-eight samples were examined petrographically, and from these, three garnet-bearing schists and one marble were analyzed by electron microprobe to determine mineral compositions. From the microprobe data, thermobarometric calculations were carried out to determine the pressure and temperature conditions of metamorphism. The pressure of equilibration was used to estimate depth, which equates to the extent of unroofing since metamorphism. Previous studies of lower plate rocks in other areas within the region have applied petrologic methods with similar goals (Hodges and Walker, 1990; Hoisch and Simpson, 1993; Holm and Wernicke, 1990; Holm and others, 1992).

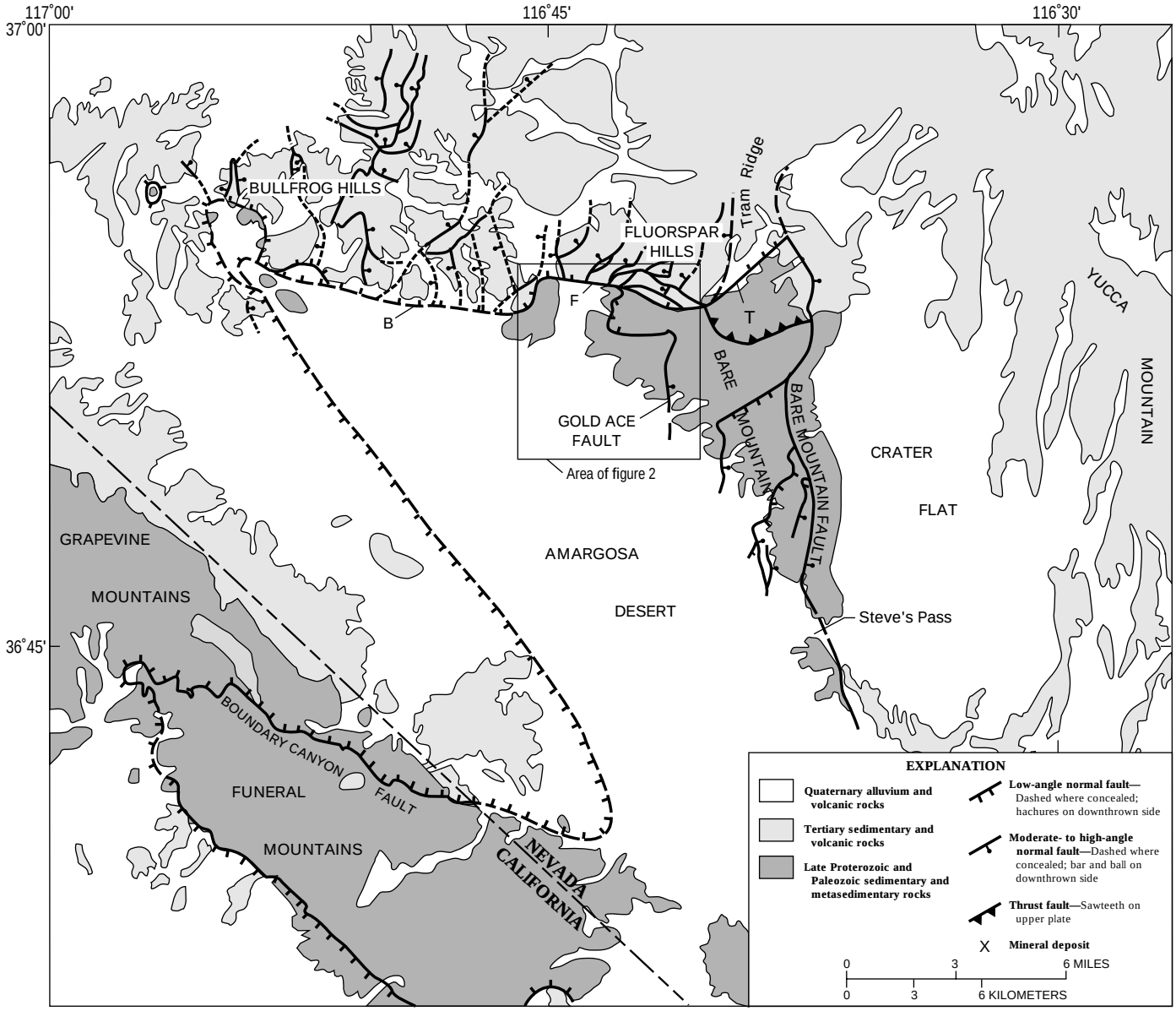


**Figure 1.** Simplified geology of Bare Mountain and surrounding areas, and locations of features mentioned in the text. Major upper-plate normal faults are shown for only Fluorspar Hills and Bullfrog Hills. Major lower-plate faults at Bare Mountain are shown. Based on Cornwall and Kleinhampl (1961), Frizzell and Shulters (1990), Maldonado (1990), Maldonado and Hausback (1990), Monsen and others (1992), Wright and Troxel (1993), and L.A. Wright (Pennsylvania State University, written commun., 1994). B, Bullfrog detachment fault; F, Fluorspar Canyon fault; T, Tates Wash fault.

## Acknowledgments

I thank F.S. Spear for discussions on the use of his computer programs, and W.B. Hamilton, C.J. Fridrich, and F.W. Simonds for their valuable insights into the geology of Bare Mountain and the tectonics of the region. I also thank Ed DeWitt, W.B. Hamilton, and M.L. Wells for helpful comments on the manuscript. J. Harvey, M. Owens, P. Sheaffer, and F.W. Simonds provided able assistance in the field and J.H. Wittke performed the microprobe analyses.

## General Geology of Bare Mountain

A gently north dipping detachment fault, the Fluorspar Canyon fault, flanks the northern margin of Bare Mountain and juxtaposes Miocene volcanic rocks in the upper plate and a thick, variably metamorphosed sequence of upper Precambrian and Paleozoic strata in the lower plate. Within the lower plate, mapping by Monsen and others (1992) showed several kinds of faults, including thrust faults, low-angle normal faults, and high-angle normal faults (fig. 1).

The highest grade of metamorphism in the lower plate, lower amphibolite facies, occurs in a fault-bounded block in the northwest corner of Bare Mountain (Monsen, 1979). The block is bounded on the north by the Fluorspar Canyon fault and on the east by an east-dipping normal fault, the Gold Ace fault. The rocks within the block are schists, semischists, and minor marble derived from Middle Cambrian and older Cambrian strata (fig. 2). Within the block, metamorphic grade and grain size decrease to the southeast. In the higher grade north half, the Wood Canyon Formation contains the mineral assemblage quartz+chlorite+muscovite+biotite+plagioclase±garnet±staurolite. Three kilometers south of the Fluorspar Canyon fault within the block, an isograd delineates the southern limit of garnet and staurolite in the Wood Canyon Formation (fig. 2).

A metamorphic grade discordance occurs across the Gold Ace fault. In one location, the grade discordance is documented by schists of the Wood Canyon Formation in the footwall juxtaposed against fossiliferous Dunderberg Shale Member of the Nopah Formation, which is not visibly metamorphosed, in the hanging wall. Conodont color-alteration indexes from hanging-wall rocks indicate conditions of middle greenschist to subgreenschist facies (Grow and others, 1994). The hanging wall consists of Middle Cambrian and younger Paleozoic rocks (fig. 2). The metamorphic grade discordance suggests a component of normal displacement greater than the ≈2,000 m of stratigraphic omission that occurs across the fault. (See section, "North-Central, Northeastern, and Eastern Bare Mountain.")

The age of the metamorphism has not been determined at Bare Mountain. However, two studies in the Funeral Mountains, located 20 km southwest of Bare Mountain (fig. 1), concluded that metamorphism in the lower plate of the detachment, there called the Boundary Canyon fault, was Early Cretaceous in age (Applegate, 1994; DeWitt and others, 1988).

## Higher Grade Rocks of the Metamorphosed Block

Garnet schists and siliceous metadolomites were sampled extensively from the northern part of the metamorphosed block, north of the garnet-staurolite isograd. These rock types provided the best potential for quantitatively determining the conditions of metamorphism.

### Mica Schists

Samples of mica schists were collected primarily from the Wood Canyon Formation in Conejo Canyon, Dry Canyon, and the Amargosa Narrows area (fig. 2). Two schists (samples 47a and 47b) were collected from the Carrara Formation on the south side of Fluorspar Canyon. Samples from the Wood Canyon Formation are fine-grained semischists containing generally 40–60 percent quartz. The primary mineral assemblage is quartz+muscovite+biotite+chlorite±plagioclase±garnet±staurolite (table 1). No sample contained more than 2 percent garnet or 2 percent staurolite. Both primary and secondary chlorite are present in most samples, the primary chlorite grains being idioblasts. Most rocks are substantially altered, with secondary chlorite replacing biotite and garnet, sericite and (or) chlorite replacing staurolite, and sericite replacing plagioclase. Unaltered pyrite was found in samples 50a and 50b, and euhedral pseudomorphs of hematite after pyrite are widespread. Pyrite grain boundaries truncate the foliation, indicating that pyrite growth was posttectonic and that sulfurous fluids pervaded the area after the development of the schistosity. Locally abundant quartz veins and hematite veins are present in Conejo Canyon and may represent manifestations of the same hydrothermal system which caused the mineral alterations.

#### Mineral Reactions and Isograds

The primary mineral assemblage quartz+muscovite+biotite+chlorite+garnet+staurolite, found in several samples (table 1*A*), indicates a reaction in which garnet and chlorite are consumed to produce staurolite and biotite as temperature increases (fig. 3). If the garnet contains significant spessartine (Mn) and (or) grossular (Ca) components, the reaction will take place through a temperature interval rather than at a specific temperature. Within that interval, as temperature increases, the proportion of staurolite+biotite to garnet+chlorite increases.

The temperature at which the reaction begins depends partly on the garnet composition; the more enriched the garnet is in Ca and Mn, the higher the temperature. The reaction ceases when one of the reactants has been exhausted. For

**Figure 2 (facing page).** Simplified geologic map of northwestern Bare Mountain; based on Monsen and others (1992) with minor reinterpretation of faults. Numbered localities refer to sample numbers in table 1.

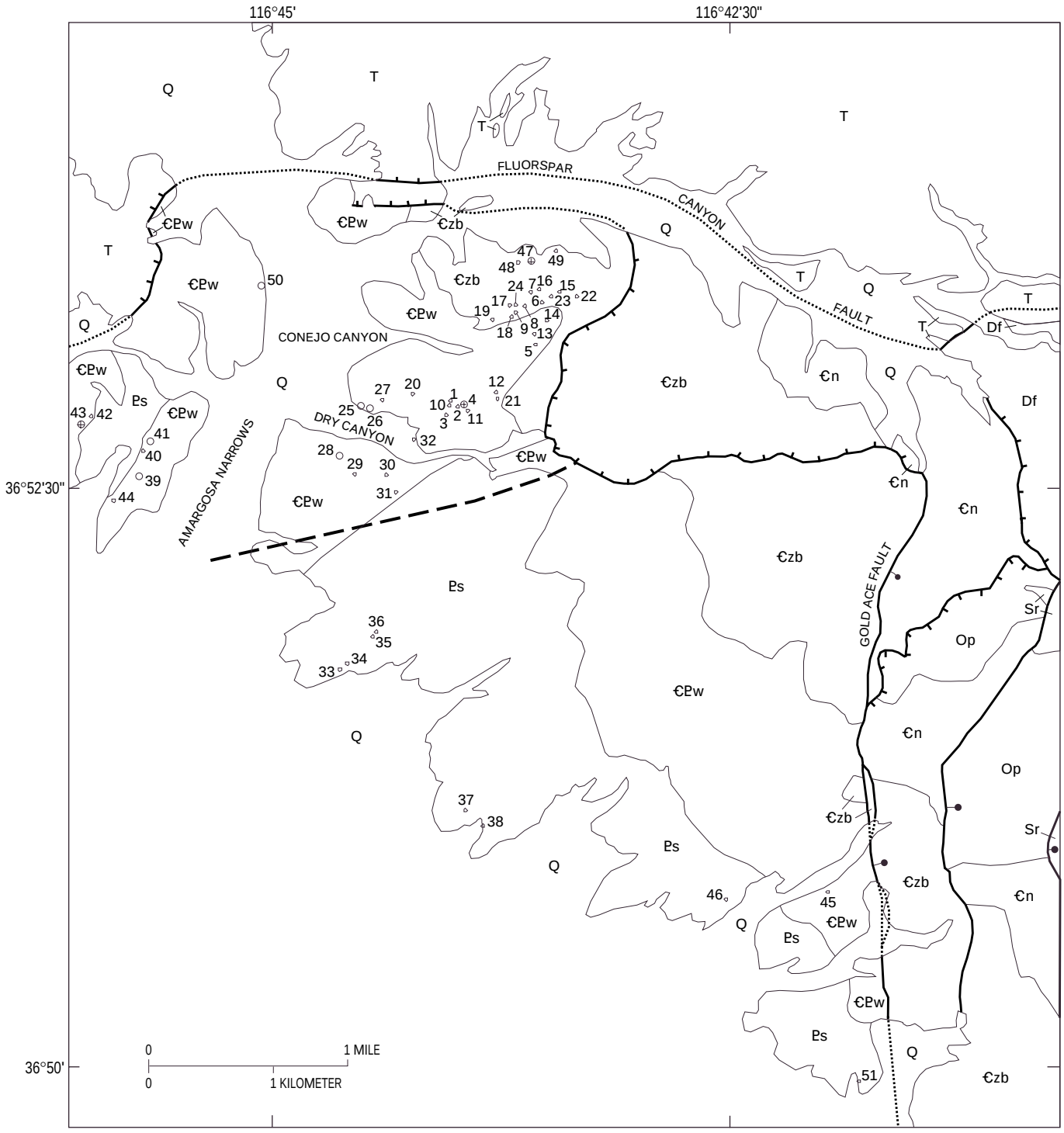


**EXPLANATION**

- Q — **Alluvium (Quaternary)**
- T — **Tuff units (Miocene)**
- Df — **Fluorspar Canyon Formation (Devonian)**
- Sr — **Roberts Mountains Formation (Silurian)**
- Op — **Pogonip Group (Ordovician)**
- €n — **Nopah Formation (Cambrian)**
- €zb — **Bonanza King and Carrara Formations, and Zabriskie Quartzite (Cambrian)**
- €Pw — **Wood Canyon Formation (Cambrian and Late Proterozoic)**
- Ps — **Sterling Quartzite (Late Proterozoic)**

**Contact**

**Garnet-staurolite isograd**

**EXTENSIONAL FAULTS**

**Covered extensional fault**

**Low-angle normal fault—**Hachures on downthrown side

**Moderate to steep-angle normal fault—** Bar and ball on downthrown side

**SAMPLE STATIONS**

⊕ **Garnet mica schist**

○ **Garnet staurolite mica schist**

◦ **Other**

**Table 1*A*.** Mineral assemblages in mica schists from northwestern Bare Mountain.

[Ap, apatite; Bio, biotite; Chte, chlorite; Ep, epidote; Gar, garnet; Hm, hematite; Ilm, ilmenite; Mag, magnetite; Mus, muscovite; Qz, quartz; Plag, plagioclase; Pyr, pyrite; Ser, sericite; St, staurolite; Tour, tourmaline; Zir, zircon. Chte(Bio) indicates a partial or complete alteration of biotite to chlorite, for example; x, present; -, not present]

| Sample No. | Qz | Mus | Bio | Gar | St | Chte | Plag | Ep | Accessory minerals | Alteration products |
|---|---|---|---|---|---|---|---|---|---|---|
| 1 | x | x | x | - | - | x | x | - | Tour, Ilm | Chte(Bio), Hm(Pyr) |
| 4a | x | x | x | - | - | x | x | - | Ilm, Zir, Tour | Chte(Bio), Hm(Pyr) |
| 4b | x | x | x | x | - | x | x | - | Ilm, Tour | Chte(Bio), Hm(Pyr) |
| 4c | x | x | x | x | x | x | x | - | Ilm, Tour | Chte(Bio), Ser(St) |
| 4d | x | x | x | x | - | x | x | - | Ilm | Chte(Bio), Hm(Pyr) |
| 11 | x | x | x | - | - | x | x | - | Tour, Ap, Zir | Chte(St), Ser(St), Chte(Bio) |
| 20a | x | x | x | - | - | - | x | x | - | Hm(Pyr) |
| 20b | x | x | x | - | - | - | x | x | Mag | - |
| 25 | x | x | x | x | - | x | x | - | Mag, Tour, Ap, Ilm | Chte(Bio |
| 26a | x | x | x | x | - | x | x | - | Mag, Tour, Ilm | Chte(Bio) |
| 26b | x | x | x | x | - | x | x | - | Tour, Mag, Ilm | Hm(Pyr), Chte(Bio), Ser(Plag) |
| 28a | x | x | x | x | - | x | x | x | Tour, Zir | Chte(Bio) |
| 28b | x | x | x | x | - | x | x | - | Tour, Mag | Chte(Bio), Chte(Gar) |
| 28c | x | x | x | - | - | - | - | - | Mag | Chte(Bio) |
| 31 | x | x | x | - | - | x | x | - | Tour, Mag, Ilm | Chte(Bio), Hm |
| 38 | x | x | x | - | - | - | - | - | - | Hm(Pyr) |
| 39a | x | x | x | x | - | x | x | x | Tour, Mag, Ilm | Chte(Gar), Chte(Bio) |
| 39b | x | x | x | x | - | x | x | - | Tour, Mag, Ilm | Chte(Bio) |
| 41 | x | x | x | x | - | x | x | x | Tour, Ilm | Hm(Pyr), Chte(Bio), Ser(Plag) |
| 43a | x | x | x | x | x | x | x | - | Tour, Mag, Ilm, Zir | Ser(St), Chte(Gar, Chte(Bio) |
| 43b | x | x | x | x | x | x | x | - | Tour, Mag, Ilm | Ser(St), Chte(Gar), Chte(Bio) |
| 45a | x | x | x | - | - | x | - | - | Tour, Mag | Hm(Pyr) |
| 47a | x | x | x | - | - | x | x | - | - | Chte(Bio), Chte(Gar) |
| 47b | x | x | x | x | x | x | x | - | Tour, Mag | Chte(Bio), Chte(Gar), Chte(St) |
| 50a | x | x | x | x | - | x | x | - | Ilm, Zir | Hm(Pyr) |
| 50b | x | x | x | x | - | x | x | - | - | Hm(Pyr) |
| 50c | x | x | x | x | - | x | x | - | Ilm, Tour | Chte(Bio), Hm(Pyr) |
| 50d | x | x | x | x | - | x | x | - | Tour | Chte(Bio) |
| 50e | x | x | x | x | - | x | x | - | Ilm, Mag, Tour | Hm(Pyr) |
| 51 | x | x | x | - | - | - | - | - | - | - |

samples 26b, 39b, and 50d, the sum of measured grossular plus spessartine components ($X_{gr} + X_{sp}$) at the garnet rim ranges from 0.190 to 0.233 (table 2*A*), which approximates the 0.2 isopleth in figure 3 (based on Spear and Cheney, 1989). Because these samples lack staurolite, the 0.2 isopleth represents an upper temperature limit. Garnet in staurolite-bearing samples may be inferred to possess lower sums of $X_{gr} + X_{sp}$ than garnet in staurolite-absent samples because lower sums would cause the reaction to initiate at lower temperatures. Thus, variations in garnet composition account for the intermixture of garnet-staurolite-chlorite and garnet-chlorite assemblages (fig. 2).

There are good reasons to suspect that the isopleths shown in figure 3 are placed at temperatures that are too high. Their placement implies that garnet-chlorite assemblages should be common in sillimanite-zone metamorphic rocks, but this is not the case. Shifting the isopleths down in temperature by 50°C would place them in a position that is more consistent with observed mineral assemblages. Two sources of uncertainty may explain the excessively high temperatures: (1) uncertainties in the thermodynamic mineral data used to calculate the curves, especially with regard to staurolite; and (2) uncertainties in the assumed composition of fluid in equilibrium with the minerals. The calculations assumed a pure water composition; however, contamination by $CO_2$ would shift isopleths to lower temperatures.

Garnet in Wood Canyon Formation grew by way of the approximate reaction chlorite + quartz = garnet + $H_2O$. Garnet growth can be understood by simulating this reaction in two ways. First, the changes in pressure and temperature associated with the zoning profiles of five different garnets were numerically simulated using the Gibbs method of Spear (1988, 1989, 1993). Second, the Gibbs method was used to define the field of pressure and temperature conditions under which garnet in one sample might have grown while chlorite was being consumed. To set up both types of models, mineral compositions at the time garnet growth began are needed. The measured compositions for plagioclase and biotite (table 2*A*) were assumed to be good approximations, even though these actually represent compositions following garnet growth, assuming no retrograde modification. The presence of only a small amount of garnet in the rock, 2 percent by volume, indicates that the reaction progressed to only a small degree and was accompanied by only small changes in mineral compositions. The garnet core composition is taken to be that of the first garnet to

**Table 1*B*.** Mineral assemblages in metacarbonate rocks from northwestern Bare Mountain.

[Bio, biotite; Chte, chlorite; Cc, calcite; Dol, dolomite; Ep, epidote; Hm, hematite; Ksp, K-feldspar; Mag, magnetite; Mus, muscovite; Qz, quartz; Phl, phlogopite; Plag, plagioclase; Pyr, pyrite; Sph, sphene; Tr, tremolite; Tour, tourmaline; Zir, zircon. Under "Alteration products" Hm(Pyr) indicates a partial or complete alteration of pyrite to hematite, for example. Other secondary phrases are also listed in this category. x, present; -, not present]

| Sample No. | Cc | Dol | Qz | Phl | Mus | Tr | Chte | Plag | Ksp | Ep | Accessory minerals | Alteration products |
|---|---|---|---|---|---|---|---|---|---|---|---|---|
| 2 | x | x | x | - | - | - | - | - | - | - | - | - |
| 3a | x | x | x | x | - | - | - | - | - | - | - | Hm(Pyr) |
| 3b | - | x | x | - | x | - | - | - | - | - | - | - |
| 3c[1] | - | x | x | - | x | - | - | - | - | - | - | Hm(Pyr) |
| 3c[1] | x | x | x | - | x | - | - | - | - | - | - | - |
| 5 | x | x | x | - | - | - | - | - | - | - | Mag | - |
| 6a | x | - | x | x | - | - | x | - | - | - | - | - |
| 6b | x | x | x | x | - | - | - | - | - | - | - | - |
| 7a | x | - | x | x | x | - | - | - | - | - | - | - |
| 7b | x | - | x | x | - | - | - | - | - | - | - | - |
| 8 | x | - | x | x | - | - | - | - | - | - | - | - |
| 9 | x | x | x | x | - | - | - | - | - | - | - | - |
| 10a | - | x | x | x | - | - | - | - | - | - | - | - |
| 10b | x | x | x | - | - | - | - | - | - | - | - | - |
| 10c | x | x | x | x | - | - | - | - | - | - | - | Hm(Pyr) |
| 10d | x | x | x | x | - | - | - | - | - | - | - | - |
| 10e | x | x | x | - | - | - | - | - | - | - | - | Hm(Pyr) |
| 12a | x | x | x | - | - | - | - | - | - | - | - | Hm(Pyr) |
| 12b | x | x | x | - | - | - | - | - | - | - | - | Hm(Pyr) |
| 12c | x | x | x | x | - | - | x | - | - | - | - | - |
| 13 | x | - | x | x | - | - | - | - | x | - | - | - |
| 14 | x | - | x | x | - | - | - | - | - | - | - | - |
| 15 | x | x | x | x | - | - | - | - | - | - | - | Hm(Pyr) |
| 16 | x | x | x | x | x | - | - | - | - | - | - | - |
| 17 | x | - | - | - | - | - | - | - | x | - | - | - |
| 18a | x | - | x | - | x | - | - | - | - | - | - | Hm(Pyr) |
| 18b | x | x | x | - | x | - | x | - | - | - | - | - |
| 19 | x | x | x | x | - | - | x | - | - | - | - | - |
| 21a | x | x | x | x | - | - | - | - | - | - | Mag | - |
| 21b | x | x | x | x | - | - | - | x | - | - | - | Hm(Pyr) |
| 22a | x | x | - | - | - | - | - | - | - | - | - | - |
| 22b | - | x | - | - | - | - | - | - | - | - | - | - |
| 23a | x | - | x | - | x | - | - | - | - | - | - | - |
| 23b | x | - | x | Bio[2] | x | - | - | - | - | - | - | - |
| 24 | x | - | x | - | - | - | - | - | - | - | - | - |
| 27a | x | - | x | Bio[2] | x | - | x | - | - | - | - | Hm(Pyr) |
| 27b | x | - | x | Bio[2] | x | - | x | - | - | - | - | Hm(Pyr) |
| 27c | x | x | - | Bio[2] | x | - | x | - | - | - | - | Hm(Pyr) |
| 29 | x | - | x | Bio[2] | x | - | x | - | - | - | - | - |
| 30a | x | - | x | Bio[2] | - | x | x | - | - | - | Sph | - |
| 30b | x | - | x | Bio[2] | - | x | - | - | - | - | Sph | - |
| 32 | x | - | x | - | x | - | - | - | - | - | - | - |
| 33 | x | x | x | Bio[2] | x | - | - | x | - | - | - | - |
| 34 | x | - | x | Bio[2] | - | x | - | - | - | - | - | Hm(Pyr) |
| 35 | - | x | x | x | - | - | - | x | x | - | Zir, Tour | Hm(Pyr) |
| 36a | x | - | x | Bio[2] | - | - | - | - | - | - | - | - |
| 36b | x | - | x | Bio[2] | - | - | - | - | - | - | - | - |
| 37a | x | x | x | Bio[2] | x | - | x | x | - | - | - | - |
| 37b | x | x | x | Bio[2] | x | - | x | x | - | - | - | - |
| 40 | x | x | x | Bio[2] | x | - | - | - | - | - | - | - |
| 42 | x | - | x | - | x | - | - | - | - | - | - | - |
| 44 | x | - | x | - | x | - | - | - | x | x | - | - |
| 45b | x | x | x | x | - | - | - | x | - | - | - | - |
| 46a | - | x | x | Bio[2] | x | - | - | - | - | - | - | Hm |
| 46b | - | x | x | - | x | - | - | x | - | - | - | - |
| 46c | - | x | x | - | x | - | x | - | - | | Zir | - |
| 48a | x | - | x | Bio[2] | x | - | - | - | - | - | - | Hm |
| 48b | x | x | - | Bio[2] | x | - | x | - | - | - | - | - |
| 49 | x | - | x | Bio[2] | - | - | - | - | - | - | - | - |

[1]Two sections of 3c were cut.

[2]Visibly pleochroic, although some are very weakly colored.

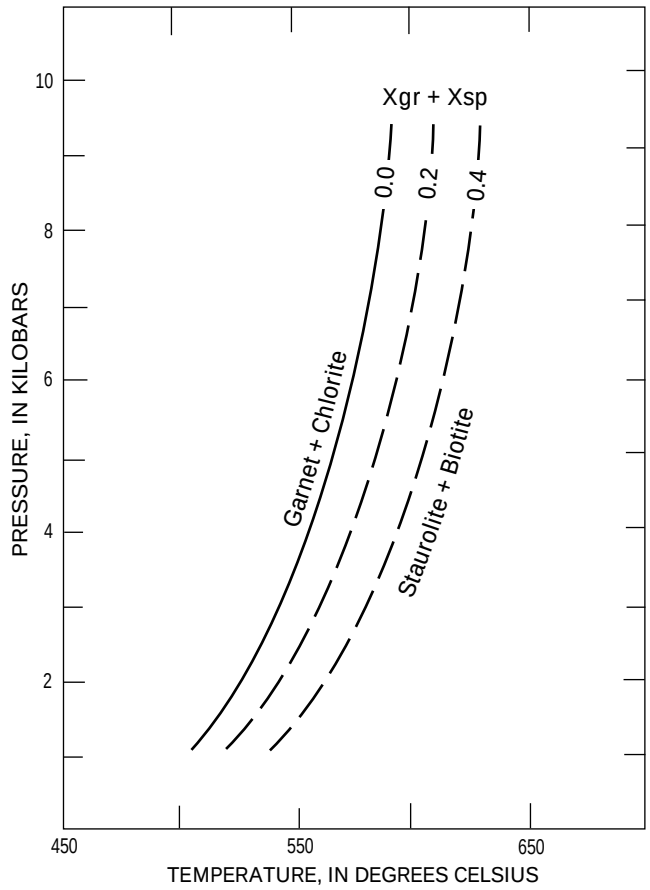


**Figure 3.** Stability diagram of coexisting quartz+muscovite+chlorite+biotite+staurolite+garnet as a function of garnet composition, based on Spear and Cheney (1989). Isopleths correspond to values of Xgr + Xsp (defined in text).

crystallize. For the five garnet growth simulations, it was assumed that growth ended at 530°C and 5 kb. For defining the pressure-temperature field of garnet growth, it was assumed that growth began at 520°C at 5 kb in sample 50d. These estimates are consistent with the thermobarometry discussed in a later section. The thermodynamic data used in the calculations are also described later.

## Garnet Growth Simulations

The measured composition profiles of the garnets are shown in figure 4. The profiles are symmetrical and smooth but vary in curvature. Generally, Mn decreases from core to rim, Fe and Mg increase, and Ca is constant or decreases slightly. The flattest profile is from the garnet in sample 39b, which yielded rim-minus-core values of $\Delta X_{py}$=0.012, $\Delta X_{gr}$=0.003, $\Delta X_{sp}$= –0.036, $\Delta X_{al}$=0.023, where the subscripts refer to the mole fraction of pyrope (py), almandine (al), spessartine (sp), and grossular (gr). The most curved profile is from the garnet in sample 26b, which yielded rim-minus-core values of $\Delta X_{py}$=0.032, $\Delta X_{gr}$= –0.060, $\Delta X_{sp}$= –0.063, $\Delta X_{al}$=0.092. The flatness and smoothness of profiles in samples 39b and 50d are suggestive of homogenization by volume diffusion at high grades of metamorphism (see, for example, Tracy, 1982); however, the rocks only reached conditions of lower amphibolite facies, where diffusion rates are too sluggish to have had a significant effect.

Recent advances in the modeling of garnet growth in pelitic schist (Spear, 1988, 1993; Spear and Florence, 1992) have incorporated important variables through the use of finite difference calculations, including the modal abundances of phases, compositions of the solid solution phases, initial pressure, initial temperature, nucleation density of the garnet, whether phases such as garnet and water are to be fractionated, a choice of thermodynamic data, a choice of activity models for solid solution phases, diffusion constants for garnet, and the pressure-temperature-time path. The calculations in this study were performed by the program DiffGibbs, version January 1990 (Spear and others, 1991).

Model simulations for each garnet profile are shown in figure 4. Table 3 gives the values used in the models. The average compositions of chlorite, biotite, and plagioclase, and the garnet core compositions (table 2*A–D*) were taken to represent the compositions at the time garnet growth began. Although the average compositions of chlorite, biotite, and plagioclase should reflect the compositions in equilibrium at the end of garnet growth, the changes in composition during the garnet growth simulations were found to be very small, thus making average measured compositions good approximations. In the model simulations, quartz, muscovite, and water were taken to be pure end members. Water and garnet were assumed to be fractionated as the garnet-growth reaction progressed—the water leaving the system and garnet remaining in contact with the system only on its outermost layer. At the temperatures involved in the simulations (530°C), volume diffusion in garnet has a negligible effect. In the simulations, garnet growth took place incrementally as temperatures increased at a constant pressure of 5 kb until a temperature of 530°C was reached. The measured zoning profiles are closely reproduced when growth was assumed to take place within an interval of 10°–25°C from core to rim at 5 kb (fig. 4). Running additional models showed the simulated profiles to be insensitive to the large uncertainties associated with the assumed initial pressure and temperature.

## Garnet-in, Chlorite-out Simulation

Two isopleths, garnet-in and chlorite-out, each representing zero mineral abundance, (mode) were calculated and plotted (fig. 5). The garnet-in isopleth represents the conditions along which garnet production begins. The chlorite-out isopleth represents the conditions at which all chlorite has reacted to form garnet. At 5 kb, the interval between the isopleths is 44.1°C. As conditions change between the garnet-in and chlorite-out isopleths, garnet grows as chlorite is consumed. The calculations assumed that no fractionation of minerals occurred during the reaction and that all minerals maintained homogeneity. The method of performing the calculations is described by Spear (1988, 1989, 1993).

Calculations were performed using the program Gibbs ’90, version January 1990 (Spear and others, 1991). The specified initial values and selected results for the calculation are given in tables 4 and 5. Initial modes were modified from a visual

**Table 2A.** Chemical composition of garnet cores and rims from northwestern Bare Mountain.

[Analysis by electron microprobe with 15 KeV accelerating voltage, 30nA sample current on brass, 5μm spot diameter and $5\times10^{-6}$ torr vacuum. Definitions: $X_{py}$, mole fraction pyrope; $X_{gr}$, mole fraction grossular; $X_{sp}$, mole fraction spessartine; $X_{al}$, mole fraction almandine. F0 and F1 refer to different areas on the polished section of sample 50d from which analyses were made. The oxidation state of Fe was determined by simultaneously solving for formulas with 8 cations and 12 oxygens]

| Analysis of.... | F1 core 1-2 | F1 rim 1 | F1 rim 2 | F0 core 4-3 | F0 rim 3 | F0 rim 4 |
|---|---|---|---|---|---|---|
| | | | **Weight percents of the oxides** | | | |
| Average of.... | 2 | 4 | 1 | 3 | 7 | 4 |
| MgO | 3.12 | 3.33 | 3.64 | 3.41 | 3.63 | 3.47 |
| $Al_2O_3$ | 21.50 | 21.34 | 21.36 | 21.64 | 21.82 | 21.52 |
| $SiO_2$ | 39.43 | 38.69 | 38.78 | 38.20 | 38.03 | 37.51 |
| CaO | 3.24 | 2.12 | 2.80 | 3.20 | 2.62 | 2.76 |
| $TiO_2$ | 0.08 | 0.02 | 0.00 | 0.09 | 0.03 | 0.02 |
| MnO | 7.81 | 5.51 | 5.63 | 7.14 | 5.35 | 5.26 |
| FeO | 28.01 | 29.45 | 30.50 | 28.28 | 30.25 | 29.83 |
| $Fe_2O_3$ | 0.00 | 0.00 | 0.00 | 0.59 | 0.24 | 0.38 |
| **Total** | 103.18 | 100.45 | 102.71 | 102.55 | 101.97 | 100.75 |
| | | | **Formulas** | | | |
| Mg | 0.36 | 0.39 | 0.42 | 0.40 | 0.43 | 0.41 |
| Al | 1.96 | 1.99 | 1.96 | 1.99 | 2.02 | 2.02 |
| Si | 3.05 | 3.06 | 3.02 | 2.98 | 2.98 | 2.98 |
| Ca | 0.27 | 0.18 | 0.23 | 0.27 | 0.22 | 0.24 |
| Ti | 0.01 | 0.00 | 0.00 | 0.01 | 0.00 | 0.00 |
| Mn | 0.51 | 0.37 | 0.37 | 0.47 | 0.36 | 0.35 |
| $Fe^{2+}$ | 1.81 | 1.95 | 1.99 | 1.85 | 1.98 | 1.98 |
| $Fe^{3+}$ | 0.00 | 0.00 | 0.00 | 0.04 | 0.01 | 0.02 |
| $X_{py}$ | 0.122 | 0.136 | 0.140 | 0.133 | 0.142 | 0.138 |
| $X_{gr}$ | 0.091 | 0.062 | 0.078 | 0.090 | 0.074 | 0.079 |
| $X_{sp}$ | 0.173 | 0.128 | 0.123 | 0.158 | 0.119 | 0.119 |
| $X_{al}$ | 0.614 | 0.675 | 0.659 | 0.619 | 0.665 | 0.665 |

estimate by setting garnet to zero and proportionally increasing everything else (table 4). The results shown in table 5 indicate that garnet growth takes place by way of the reaction: quartz+chlorite=garnet+$H_2O$, with very little participation of plagioclase, muscovite, or biotite.

## Thermodynamic Data

For the calculation of constant-mode isopleths (fig. 5 and tables 4 and 5) and garnet growth simulations (fig. 4 and table 3), thermodynamic data for pure phases and end-member components in solid solution are from Berman (1988a), except for the end-member components of chlorite (Fe-Mg-Mn) and for spessartine. Data for water are from Haar and others (1984). Thermodynamic data for the Mg-end member of chlorite [$Mg_{4.7}Al_{2.6}Si_{2.7}O_{10}(OH)_8$] were created by the oxide exchange method of Holland (1989) using Berman's (1988a) clinochlore [$Mg_5Al_2Si_3O_{10}(OH)_8$] as the basis component. Thermodynamic data for the Fe- and Mn-end members were then calculated from the new Mg-chlorite data using Berman's (1988b) Mg-Fe and Mg-Mn exchange values. Spessartine data were calculated using Berman's (1988b) Fe-Mn exchange values applied to almandine data from Berman (1988a). All these calculations were performed using the program Make Thermo File by F.S. Spear. Heat-capacity data were calculated for chlorite (all components) and spessartine using expression (1) from Berman and Brown (1985). Expansivities and compressibilities for chlorite and spessartine were taken from Powell and Holland (1985).

## Thermobarometry

Samples suitable for thermobarometry contain the mineral assemblage quartz+muscovite+garnet+plagioclase+biotite +chlorite, to which the 43 barometers of Hoisch (1991), the garnet-biotite geothermometer (Hodges and Spear, 1982), and the garnet-chlorite geothermometer (Grambling, 1990) can be applied. Mineral assemblages suitable for other barometers commonly applied to pelitic schist, such as garnet+$Al_2SiO_5$+quartz+plagioclase (Newton and Haselton, 1981) or garnet+rutile+$Al_2SiO_5$+ilmenite (Bohlen and others, 1983), were not found because bulk compositions were not proportionally high enough in Al to crystallize any $Al_2SiO_5$ phase.

In selection of mineral compositions for thermobarometric calculations, considering what will best represent equilibrium is important. The preservation of growth zoning in garnet suggests that the rims are in equilibrium with the matrix phases. The

**Table 2A.** Chemical composition of garnet cores and rims from northwestern Bare Mountain—*Continued.*

[Analysis by electron microprobe with 15 KeV accelerating voltage, 30nA sample current on brass, 5μm spot diameter and $5\times10^{-6}$ torr vacuum. Definitions: $X_{py}$, mole fraction pyrope; $X_{gr}$, mole fraction grossular; $X_{sp}$, mole fraction spessartine; $X_{al}$, mole fraction almandine. F0 and F1 refer to different areas on the polished section of sample 50d from which analyses were made. The oxidation state of Fe was determined by simultaneously solving for formulas with 8 cations and 12 oxygens]

| Analysis of.... | F0 core 5-6 | F0 rim 5 | F0 rim 6 | 26b rim 1 | 26b rim 2 | 26b rim 3 |
|---|---|---|---|---|---|---|
| **Weight percents of the oxides** | | | | | | |
| Average of.... | 4 | 6 | 3 | 8 | 1 | 1 |
| MgO | 3.39 | 3.46 | 2.92 | 3.52 | 2.96 | 3.37 |
| $Al_2O_3$ | 21.46 | 21.68 | 21.38 | 21.04 | 21.53 | 21.84 |
| $SiO_2$ | 38.17 | 38.99 | 38.28 | 37.14 | 37.39 | 36.94 |
| CaO | 3.14 | 2.52 | 2.74 | 2.59 | 2.58 | 3.74 |
| $TiO_2$ | 0.06 | 0.04 | 0.04 | 0.04 | 0.00 | 0.02 |
| MnO | 7.36 | 5.40 | 5.59 | 4.95 | 5.63 | 5.39 |
| FeO | 28.18 | 30.29 | 30.20 | 29.11 | 30.43 | 27.93 |
| $Fe_2O_3$ | 0.77 | 0.00 | 0.00 | 0.00 | 1.21 | 2.51 |
| **Total** | 102.53 | 102.38 | 101.15 | 98.39 | 101.73 | 101.74 |
| **Formulas** | | | | | | |
| Mg | 0.40 | 0.40 | 0.34 | 0.43 | 0.35 | 0.40 |
| Al | 1.98 | 1.99 | 1.99 | 2.01 | 2.01 | 2.03 |
| Si | 2.99 | 3.04 | 3.03 | 3.01 | 2.96 | 2.91 |
| Ca | 0.26 | 0.21 | 0.23 | 0.23 | 0.22 | 0.32 |
| Ti | 0.00 | 0.00 | 0.00 | 0.00 | 0.00 | 0.00 |
| Mn | 0.49 | 0.36 | 0.37 | 0.34 | 0.38 | 0.36 |
| $Fe^{2+}$ | 1.84 | 1.97 | 2.00 | 1.97 | 2.01 | 1.84 |
| $Fe^{3+}$ | 0.05 | 0.00 | 0.00 | 0.00 | 0.07 | 0.15 |
| $X_{py}$ | 0.132 | 0.137 | 0.117 | 0.143 | 0.118 | 0.136 |
| $X_{gr}$ | 0.088 | 0.071 | 0.079 | 0.076 | 0.074 | 0.109 |
| $X_{sp}$ | 0.163 | 0.121 | 0.127 | 0.115 | 0.127 | 0.124 |
| $X_{al}$ | 0.617 | 0.671 | 0.676 | 0.666 | 0.681 | 0.632 |

compositions of muscovite, biotite, and chlorite show no systematic variation between cores and rims. Plagioclase grains are generally small (<30 μm for the longest dimension) and unzoned. Thus, equilibrium was assumed to be represented by the composition of garnet rims and average compositions for biotite, chlorite, muscovite, and plagioclase.

The results of garnet-biotite geothermometry indicate that the composition of the biotite is inconsistent with equilibrium. Twelve determinations of temperature range from 613°±50°C to 762°±50°C (average 687°C, table 6). These temperatures represent upper amphibolite or granulite facies conditions, which are inconsistent with the predicted stability of chlorite (fig. 5), with the mineral assemblages and geothermometry in metacarbonate rocks (discussed in section, "Siliceous Metadolomite"), and with the preservation of growth zoning in garnet. Temperatures calculated using the garnet-chlorite geothermometer vary from 530°±50°C to 593°±50°C (average 570°C, table 6) and are more consistent with these characteristics but still probably a little too high. The indicated uncertainty of ±50°C is derived from the propagation of analytical errors (2σ) and should be regarded as a minimum expression of uncertainty in the temperature.

The erroneously high temperatures calculated from garnet-biotite and garnet-chlorite pairs reflect anomalously high Fe/Mg ratios in biotite and chlorite relative to garnet. Iron enrichment of biotite and chlorite was found to be a product of retrogradation in similar rocks studied by Florence and Spear (1993), who also obtained anomalously high calculated temperatures. They (Florence and Spear, 1993) found that the retrogradation was a result of interaction with a hydrothermal fluid at temperatures below the peak of metamorphism. The retrograde reaction involves garnet consumption: garnet+$H_2O$=chlorite+quartz (the garnet-producing reaction in reverse). During the reaction, the garnet underwent Fe enrichment, but only along the outer 1–2 μm because sluggish rates of volume diffusion prevented equilibration with all but the outermost rim. In the present study, the complete reaction of garnet to chlorite would produce changes in mineral compositions that are much smaller than needed, although these changes would be in the direction of Fe-enrichment. Thus, if the system was closed with respect to cations, as in the models of Florence and Spear (1993), then retrogradation could not explain most of the Fe-enrichment observed in the present study.

The best speculation that may be offered to explain the Fe-enrichment of biotite and chlorite is that Fe from altered pyrite became mobilized by hydrothermal fluids and underwent exchange with Mg in chlorite and biotite. This could explain

**Table 2A.** Chemical composition of garnet cores and rims from northwestern Bare Mountain—*Continued.*

[Analysis by electron microprobe with 15 KeV accelerating voltage, 30nA sample current on brass, 5μm spot diameter and $5\times10^{-6}$ torr vacuum. Definitions: $X_{py}$, mole fraction pyrope; $X_{gr}$, mole fraction grossular; $X_{sp}$, mole fraction spessartine; $X_{al}$, mole fraction almandine. F0 and F1 refer to different areas on the polished section of sample 50d from which analyses were made. The oxidation state of Fe was determined by simultaneously solving for formulas with 8 cations and 12 oxygens]

| Analysis of.... | 26b rim 4 | 26b core | 39b rim3 | 39b rim 4 | 39b core |
|---|---|---|---|---|---|
| **Weight percents of the oxides** | | | | | |
| Average of.... | 1 | 4 | 1 | 1 | 3 |
| MgO | 3.49 | 2.55 | 3.44 | 3.26 | 3.08 |
| $Al_2O_3$ | 21.29 | 21.05 | 21.26 | 21.33 | 21.88 |
| $SiO_2$ | 36.86 | 36.99 | 38.69 | 38.00 | 38.73 |
| CaO | 2.44 | 4.65 | 3.43 | 3.56 | 3.42 |
| $TiO_2$ | 0.11 | 0.15 | 0.10 | 0.11 | 0.08 |
| MnO | 5.22 | 8.05 | 4.26 | 4.21 | 5.91 |
| FeO | 29.54 | 25.72 | 30.09 | 30.90 | 29.81 |
| $Fe_2O_3$ | 1.04 | 0.32 | 0.00 | 0.11 | 0.00 |
| **Total** | 99.99 | 99.48 | 101.27 | 101.48 | 102.91 |
| **Formulas** | | | | | |
| Mg | 0.42 | 0.31 | 0.40 | 0.38 | 0.36 |
| Al | 2.01 | 2.00 | 1.97 | 1.98 | 2.00 |
| Si | 2.96 | 2.98 | 3.04 | 3.00 | 3.01 |
| Ca | 0.21 | 0.40 | 0.29 | 0.30 | 0.29 |
| Ti | 0.01 | 0.01 | 0.01 | 0.01 | 0.01 |
| Mn | 0.36 | 0.55 | 0.28 | 0.28 | 0.39 |
| $Fe^{2+}$ | 1.98 | 1.73 | 1.98 | 2.04 | 1.94 |
| $Fe^{3+}$ | 0.07 | 0.19 | 0.00 | 0.01 | 0.00 |
| $X_{py}$ | 0.141 | 0.102 | 0.136 | 0.128 | 0.120 |
| $X_{gr}$ | 0.071 | 0.134 | 0.098 | 0.100 | 0.096 |
| $X_{sp}$ | 0.120 | 0.184 | 0.096 | 0.094 | 0.131 |
| $X_{al}$ | 0.669 | 0.580 | 0.673 | 0.679 | 0.653 |

the Fe-enrichment of biotite and chlorite without noticeably affecting the garnet. In garnet, a narrow Fe-rich (1–2 μm) rim, too thin to be detected by the electron microprobe, would develop. Because volume diffusion in chlorite and biotite is rapid even at low-grade conditions, reequilibration would be achieved throughout the crystals. If equilibrium was attained, then the mineral compositions would be a function of the temperature of the hydrothermal interaction—the lower the temperature, the more Fe-rich the biotite, chlorite, and garnet compositions become. The Fe/Mg partitioning among the minerals would also be indicative of the equilibrium temperature. Garnet-biotite and garnet-chlorite geothermometry would give the correct temperatures if the composition of the narrow Fe-rich rim of the garnet could be determined. The presence of hematite veins in the area supports the possibility of infiltration by a hydrothermal fluid rich in dissolved Fe.

Performing the thermobarometry calculations to determine peak metamorphic conditions requires that equilibrium mineral compositions at the peak of metamorphism be known. Because the evidence points to retrograde Fe-enrichment of the biotite, a correction must be applied. Using the garnet-biotite geothermometer (Hodges and Spear, 1982) and a pressure of 5 kb, temperatures of 487°±50°C to 550°±50°C (average 530°C) were calculated when the analyzed compositions were modified by substituting 0.25 Fe with 0.25 Mg in the normalized formulas for samples 50d (F1 and F0 averages) and 26b, and substituting 0.40 Fe with 0.40 Mg for sample 39b (table 2*B*). An average temperature of 530°C was selected as a target because this approximate temperature is indicated by mineral assemblages in mica schist and siliceous metacarbonate rocks and by calcite-dolomite geothermometry (discussed in section, "Siliceous Metadolomite"). Using the modified biotite compositions and averages for garnet rims, muscovite, and plagioclase, plots of mineral equilibria were calculated (fig. 6) using the method of Hoisch (1991). Excluding the results for sample 39b, which shows particularly large scatter, a pressure of 5.3±1.5 kb is indicated. The uncertainty indicates the range of pressures at which lines representing the geobarometry equilibria cross the garnet-biotite geothermometry line (fig. 6). Analytical errors, uncertainties in activity-composition models, uncertainties associated with the calibration of the barometers, and uncertainty in the equilibrium biotite composition contribute additional uncertainty to the pressure estimate; the total uncertainty is unquantifiable but greater than 1.5 kb.

The constant-mode isopleths calculated in figure 5 used uncorrected biotite compositions. When corrected compositions

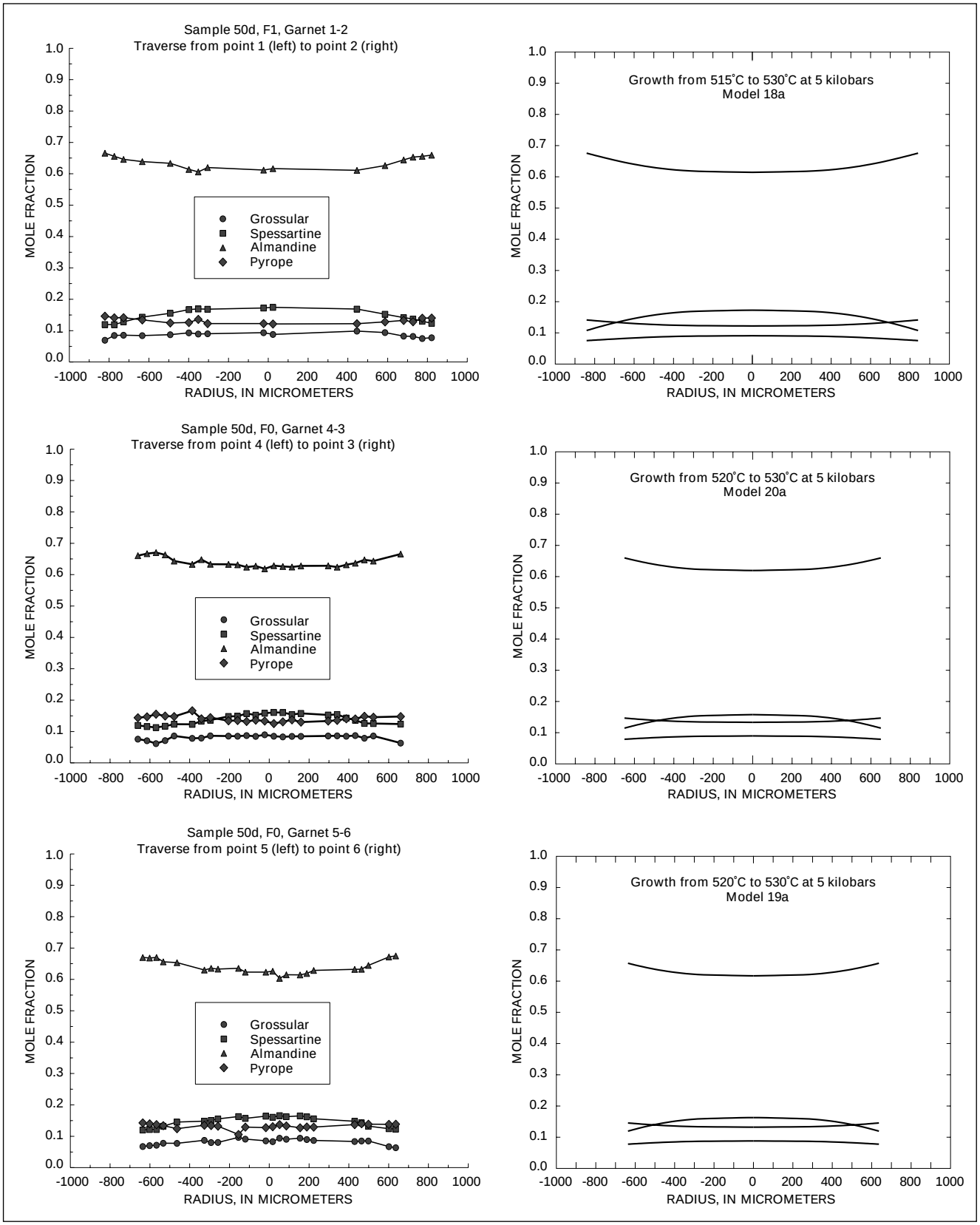


**Figure 4 (above and following page).** Garnet zoning profiles and model growth simulations. Measured profiles are on the left, simulations on the right. Specified variables and initial conditions are given in table 1*A*. Model numbers correspond to those listed in table 3.

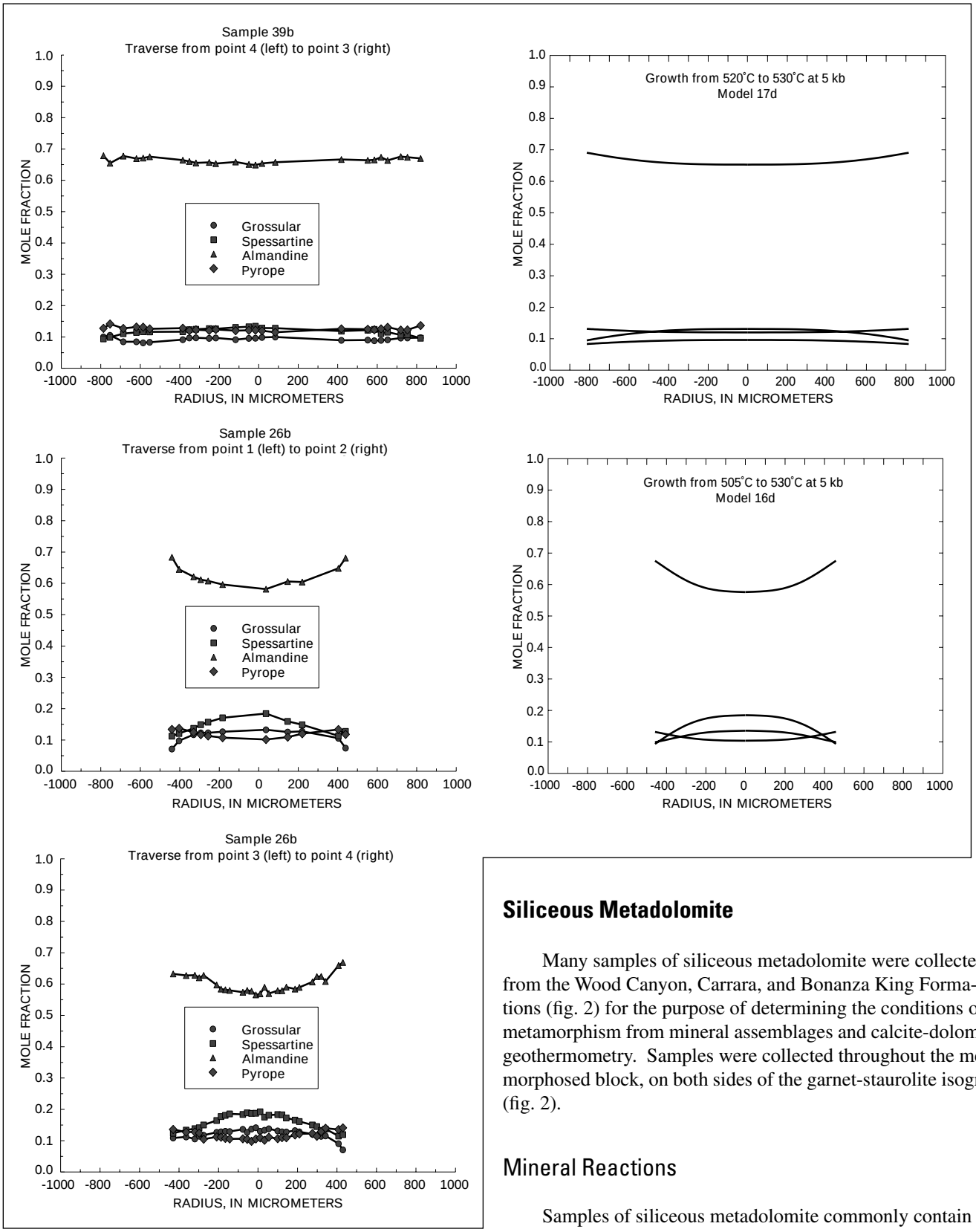


for biotite and chlorite were substituted into the models (chlorite modified +0.50 Mg and –0.50 Fe, and biotite modified +0.25 Mg and –0.25 Fe per formula), the resultant isopleths appear very similar to those shown in figure 5.

## Siliceous Metadolomite

Many samples of siliceous metadolomite were collected from the Wood Canyon, Carrara, and Bonanza King Formations (fig. 2) for the purpose of determining the conditions of metamorphism from mineral assemblages and calcite-dolomite geothermometry. Samples were collected throughout the metamorphosed block, on both sides of the garnet-staurolite isograd (fig. 2).

### Mineral Reactions

Samples of siliceous metadolomite commonly contain clinochlore, phlogopite (or weakly pleochroic biotite), muscovite, calcite, and dolomite, and less commonly, tremolite, plagioclase, and potassium feldspar (table 1*B*). No tremolite was found south of sample site 34 (fig. 2). The presence of tremolite+calcite and quartz+dolomite assemblages and the

**Table 2*B*.** Chemical composition of micas from northwestern Bare Mountain.

[Analysis by electron microprobe—see table 2*A* for run conditions. Definitions: $X_{phl}$, mole fraction phlogopite; $X_{ann}$, mole fraction annite; $X_{Mn}$, mole fraction Mn-biotite. All Fe is assumed to be $Fe^{2+}$. n/a, not applicable; mus, muscovite; bio, biotite. F0 and F1 refer to different areas on the polished section of sample 50d from which analyses were taken. Asterisks (*) indicate analyses that have been corrected for the effects of retrograde metasomatism by adding 0.25 Mg and subtracting 0.25 Fe per formula for all except 39b, which was corrected by adding 0.40 Mg and subtracting 0.40 Fe - see text for explanation. Formulas are based on normalization to 11 anhydrous oxygens]

| Analysis of.... | F1 Mus | F0 Mus | 39b Mus | 26b Mus | F1 Bio | F1Bio* |
|---|---|---|---|---|---|---|
| | | | **Weight percents of the oxides** | | | |
| Average of.... | 9 | 9 | 5 | 6 | 7 | n/a |
| $Na_2O$ | 1.08 | 1.05 | 1.00 | 1.07 | 0.18 | 0.18 |
| MgO | 0.76 | 0.85 | 0.87 | 0.81 | 10.36 | 12.86 |
| $Al_2O_3$ | 33.65 | 34.07 | 34.33 | 34.40 | 17.86 | 18.20 |
| $SiO_2$ | 49.12 | 47.50 | 46.05 | 45.69 | 38.62 | 39.34 |
| $K_2O$ | 8.50 | 8.52 | 9.63 | 9.34 | 8.86 | 9.03 |
| $TiO_2$ | 0.50 | 0.40 | 0.42 | 0.43 | 1.47 | 1.50 |
| MnO | 0.00 | 0.00 | 0.00 | 0.00 | 0.12 | 0.13 |
| FeO | 3.10 | 3.43 | 3.06 | 3.15 | 19.52 | 15.76 |
| **Total** | 96.71 | 95.82 | 95.36 | 94.89 | 96.99 | 97.00 |
| | | | **Formulas** | | | |
| Na | 0.14 | 0.13 | 0.13 | 0.14 | 0.03 | 0.03 |
| Mg | 0.07 | 0.08 | 0.09 | 0.08 | 1.14 | 1.39 |
| Al | 2.59 | 2.65 | 2.71 | 2.73 | 1.56 | 1.56 |
| Si | 3.20 | 3.14 | 3.08 | 3.07 | 2.86 | 2.86 |
| K | 0.71 | 0.72 | 0.82 | 0.80 | 0.84 | 0.84 |
| Ti | 0.02 | 0.02 | 0.02 | 0.02 | 0.08 | 0.08 |
| Mn | 0.00 | 0.00 | 0.00 | 0.00 | 0.01 | 0.01 |
| $Fe^{2+}$ | 0.17 | 0.19 | 0.17 | 0.18 | 1.21 | 0.96 |
| $X_{phl}$ | n/a | n/a | n/a | n/a | 0.485 | 0.591 |
| $X_{ann}$ | n/a | n/a | n/a | n/a | 0.512 | 0.406 |
| $X_{Mn}$ | n/a | n/a | n/a | n/a | 0.00339 | 0.00339 |

| Analysis of.... | F0 Bio | F0 Bio* | 39b Bio | 39b Bio* | 26b Bio | 26b Bio* |
|---|---|---|---|---|---|---|
| | | | **Weight percents of the oxides** | | | |
| Average of.... | 15 | n/a | 6 | n/a | 6 | n/a |
| $Na_2O$ | 0.14 | 0.14 | 0.16 | 0.17 | 0.11 | 0.11 |
| MgO | 10.47 | 12.94 | 9.64 | 13.52 | 10.47 | 12.93 |
| $Al_2O_3$ | 18.31 | 18.64 | 18.11 | 18.64 | 18.72 | 19.06 |
| $SiO_2$ | 36.96 | 37.64 | 35.26 | 36.29 | 36.41 | 37.08 |
| $K_2O$ | 9.47 | 9.64 | 9.46 | 9.74 | 9.56 | 9.74 |
| $TiO_2$ | 1.49 | 1.52 | 1.37 | 1.41 | 1.48 | 1.51 |
| MnO | 0.12 | 0.13 | 0.10 | 0.11 | 0.10 | 0.10 |
| FeO | 19.65 | 15.95 | 21.53 | 15.76 | 19.43 | 15.74 |
| **Total** | 96.61 | 96.60 | 95.63 | 95.64 | 96.28 | 96.27 |
| | | | **Formulas** | | | |
| Na | 0.02 | 0.02 | 0.02 | 0.02 | 0.02 | 0.02 |
| Mg | 1.17 | 1.42 | 1.10 | 1.50 | 1.17 | 1.42 |
| Al | 1.62 | 1.62 | 1.64 | 1.64 | 1.66 | 1.66 |
| Si | 2.77 | 2.77 | 2.71 | 2.71 | 2.74 | 2.74 |
| K | 0.91 | 0.91 | 0.93 | 0.93 | 0.92 | 0.92 |
| Ti | 0.08 | 0.08 | 0.08 | 0.08 | 0.08 | 0.08 |
| Mn | 0.01 | 0.01 | 0.01 | 0.01 | 0.01 | 0.01 |
| $Fe^{2+}$ | 1.23 | 0.98 | 1.38 | 0.98 | 1.22 | 0.97 |
| $X_{phl}$ | 0.486 | 0.589 | 0.442 | 0.603 | 0.489 | 0.593 |
| $X_{ann}$ | 0.511 | 0.407 | 0.555 | 0.394 | 0.509 | 0.405 |
| $X_{Mn}$ | 0.00332 | 0.00332 | 0.00281 | 0.00281 | 0.00250 | 0.00250 |

**Table 2C.** Chemical composition of plagioclase from northwestern Bare Mountain.

[Analysis by electron microprobe - see table 2A for run conditions. Definitions: $X_{ab}$, mole fraction albite; $X_{an}$, mole fraction anorthite. All Fe is assumed to be $Fe^{2+}$. F0 and F1 refer to different areas on the polished section of sample 50d from which analyses were taken. Formulas are based on normalization to eight anhydrous oxygens]

| Analysis of.... | F0 | F1 | 26b | 39b |
|---|---|---|---|---|
| | | **Weight percents of the oxides** | | |
| Average of.... | 8 | 9 | 13 | 4 |
| $Na_2O$ | 8.44 | 8.60 | 7.89 | 8.54 |
| $Al_2O_3$ | 24.98 | 25.27 | 24.51 | 23.22 |
| $SiO_2$ | 61.96 | 62.05 | 59.53 | 61.21 |
| $K_2O$ | 0.22 | 0.09 | 0.09 | 0.09 |
| CaO | 5.08 | 5.24 | 5.54 | 4.49 |
| FeO | 0.06 | 0.06 | 0.08 | 0.09 |
| **Total** | 100.74 | 101.31 | 97.64 | 97.64 |
| | | **Formulas** | | |
| Na | 0.72 | 0.73 | 0.70 | 0.75 |
| Al | 1.30 | 1.30 | 1.31 | 1.24 |
| Si | 2.73 | 2.72 | 2.70 | 2.77 |
| K | 0.01 | 0.01 | 0.01 | 0.01 |
| Ca | 0.24 | 0.25 | 0.27 | 0.22 |
| $Fe^{2+}$ | 0.00 | 0.00 | 0.00 | 0.00 |
| $X_{ab}$ | 0.751 | 0.748 | 0.721 | 0.775 |
| $X_{an}$ | 0.249 | 0.252 | 0.279 | 0.225 |

absence of talc and diopside provide a modest limit on the temperature of metamorphism for the area of sample site 34 and northward. The conditions of metamorphism must straddle the reaction dolomite+quartz+$H_2O$=tremolite+calcite+$CO_2$ which takes place at 520°–605°C at 5 kb (fig. 7). The range of temperatures stems from a dependence on fluid composition, which varied locally.

## Calcite-Dolomite Geothermometry

The calcite-dolomite geothermometer is based upon the Mg concentration in calcite, which varies directly with temperature when calcite coexists with dolomite. Nineteen grains of calcite in sample 40 were analyzed for calcite-dolomite geothermometry (fig. 8) using the calibration of Anovitz and Essene (1987). Calculated temperatures vary considerably: two grains fall above 560°C, eight between 510°C and 560°C, and nine below 510°C. Such variation is typical of calcite-dolomite geothermometry applications (for example, Bowman and Essene, 1982) and may result from a number of factors. If calcite that formed during prograde reactions retains its initial composition and does not reequilibrate at higher temperatures, calculated temperatures will be too low. Whether samples reequilibrate at higher temperatures is dependent upon rates of volume diffusion. As in garnet, volume diffusion in calcite is temperature-dependent. Although the temperature at which the rate becomes significant is not precisely known, the well-documented tendency of calcite to diffusionally reequilibrate during retrogradation from high-grade metamorphism (for example, Essene, 1982) implies that volume diffusion is rapid above 650°C.

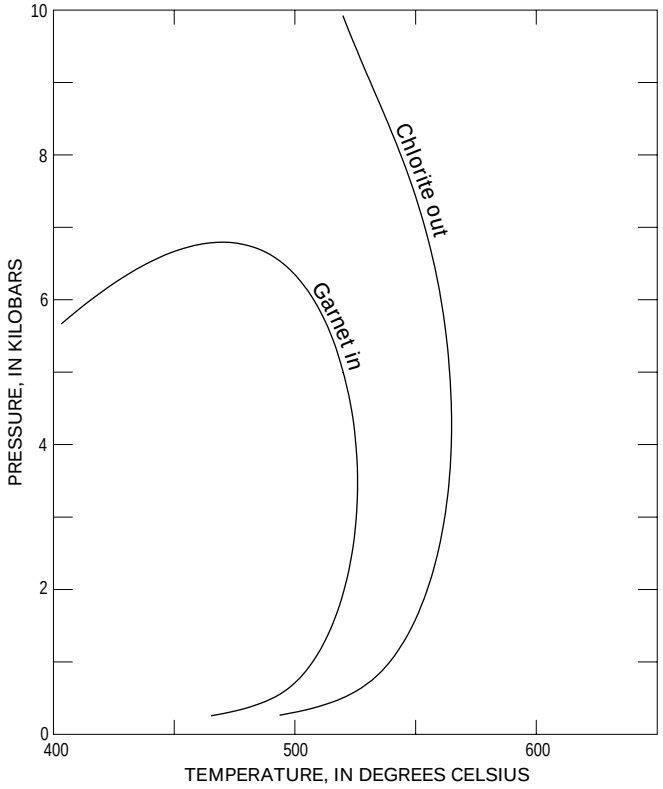


**Figure 5.** Calculated isopleths of garnet absent ("garnet in") and chlorite absent ("chlorite out") for garnet 5-6 in sample 50d from northwestern Bare Mountain. See tables 3 and 4 and discussion in text for details of the calculations.

**Table 2*D*.** Chemical composition of chlorite from northwestern Bare Mountain.

[Analysis by electron microprobe - see table 2*A* for run conditions. Definitions: $X_{clin}$, mole fraction clinochlore; $X_{daph}$, mole fraction daphnite, $X_{Mn}$, mole fraction Mn-chlorite. All Fe is assumed to be $Fe^{2+}$. Label "F1/F0" represents data that were collected from several grains outside the F1 and F0 regions of sample 50d, as these regions lacked chlorite. Formulas are based on normalization to 14 anhydrous oxygens]

| Analysis of.... | F1/F0 | 26b | 39b |
|---|---|---|---|
| **Weight percents of the oxides** | | | |
| Average of.... | 11 | 8 | 9 |
| $Na_2O$ | 0.002 | 0.01 | 0.05 |
| MgO | 16.26 | 16.38 | 16.30 |
| $Al_2O_3$ | 21.95 | 21.70 | 22.54 |
| $SiO_2$ | 26.11 | 27.38 | 26.40 |
| $K_2O$ | 0.46 | 0.45 | 0.27 |
| CaO | 0.00 | 0.06 | 0.07 |
| $TiO_2$ | 1.23 | 0.05 | 0.13 |
| MnO | 0.13 | 0.14 | 0.14 |
| FeO | 23.22 | 24.25 | 22.82 |
| **Total** | 89.34 | 90.42 | 88.72 |
| **Formula** | | | |
| Na | 0.00 | 0.00 | 0.01 |
| Mg | 2.48 | 2.47 | 2.49 |
| Al | 2.64 | 2.59 | 2.72 |
| Si | 2.67 | 2.77 | 2.71 |
| K | 0.06 | 0.06 | 0.04 |
| Ca | 0.00 | 0.01 | 0.01 |
| Ti | 0.10 | 0.00 | 0.01 |
| Mn | 0.01 | 0.01 | 0.01 |
| $Fe^{2+}$ | 1.99 | 2.05 | 1.96 |
| $X_{clin}$ | 0.554 | 0.545 | 0.559 |
| $X_{daph}$ | 0.444 | 0.453 | 0.439 |
| $X_{Mn}$ | 0.00246 | 0.00265 | 0.00269 |

When calcite undergoes retrogradation, Mg may diffuse to adjacent dolomite grains and dolomite may exsolve. Grains may also develop coherent Mg-rich and Mg-poor patches. Calcite that preserves a lower Mg content than was in equilibrium at the peak of metamorphism will result in calculated temperatures that are too low. Conversely, anomalously Mg-rich patches or areas that contain exsolved dolomite may result in calculated temperatures that are too high.

A prudent interpretation of the data in figure 8 is that the equilibrium temperature falls between 510°C and 560°C. The two temperatures above 560°C might have resulted from the analysis of Mg-rich patches or the presence of exsolved dolomite, and the nine grains below 510°C reflect either compositions inherited during progradation or the loss of Mg by diffusion during retrogradation.

## Lower Grade Rocks of the Metamorphosed Block

Samples were collected within several canyons along the western flank of central Bare Mountain south of the garnet-staurolite isograd within the metamorphosed block (fig. 2). The absence of garnet and staurolite and finer grain size in mica schists from the Wood Canyon Formation indicate a lower grade than in the northern part (table 1*A*). Similarly, mineral assemblages in siliceous metacarbonates south of sample site 34 lack tremolite (table 1*B*), which also implies a lower grade of metamorphism.

## North-Central, Northeastern, and Eastern Bare Mountain

Rocks in the hanging wall of the Gold Ace fault have the appearance of unmetamorphosed sedimentary rocks. Pelitic rocks are friable shale that breaks easily along thin bedding laminae and commonly preserves fossils. Grow and others (1994) reported 15 determinations of conodont color-alteration indexes (CAI) from Upper Cambrian to Mississippian strata. Assuming that maximum temperatures lasted $10^6$–$10^8$ years, an index value of 4 corresponds to 190°–240°C and a value of 5.5 corresponds to 350°–400°C (Rejebian and others, 1987). The two samples with the lowest values (4 and 4–4.5) are in the hanging

**Table 3.** Mineral analyses and specified values for simulations of growth in garnets from northwestern Bare Mountain.

[Thermodynamic data, activity models, and initial modes are same as model in figure 5. Analyses are from table 2]

| Model Number | 16d | 17d | 18a | 19a | 20a |
|---|---|---|---|---|---|
| | | | **Mineral analyses** | | |
| Plagioclase | 26b | 39b | F1 | F0 | F0 |
| Biotite | 26b Bio | 39b Bio | F1 Bio | F0 Bio | F0 Bio |
| Chlorite | 26b | 39b | F1/F0 | F1/F0 | F1/F0 |
| Garnet | 26b | 39b | F1 core 1-2 | F0 core 5-6 | F0 core 4-3 |
| | | | **Initial modes (volume percent) *** | | |
| α-Quartz | 45 | 30 | 48 | 48 | 48 |
| Muscovite | 2 | 54 | 26 | 26 | 26 |
| Plagioclase | 45 | 2 | 13 | 13 | 13 |
| Biotite | 6 | 12 | 11 | 11 | 11 |
| Water | 0 | 0 | 0 | 0 | 0 |
| Chlorite | 2 | 2 | 2 | 2 | 2 |
| Garnet | 0 | 0 | 0 | 0 | 0 |
| | | | **Other values** | | |
| Nucleation density (crystals/100 $cm^3$ rock) | 150 | 35 | 38 | 60 | 60 |
| Pressure (bars) | 5,000 | 5,000 | 5,000 | 5,000 | 5,000 |
| Initial temperature (°C) | 505 | 520 | 515 | 520 | 520 |
| Final temperature (°C) | 530 | 530 | 530 | 530 | 530 |
| Heating rate (°C/Ma) | 10 | 10 | 10 | 10 | 10 |

*Modified from visual estimates by setting garnet to zero and proportionally increasing the other phases. The actual percentages of garnet in samples 26b, 39b, and 50d are 1–2 percent.

wall of a thrust fault in the northeastern part of the range (fig. 1). The remaining 13 samples come from the thrust footwall a short distance west of the thrust fault and from along the east flank of the range south of the thrust fault. Samples from these areas vary from 4.5–5 to 5.5–7; most are 5.5 ± 1.0. Thus, lower temperatures were attained in the hanging wall of the thrust than in the footwall. Because rocks in the hanging wall are older strata than those in the footwall, the CAI values do not correlate with depth in the sedimentary package but are instead consistent with thermal relaxation after thrusting.

The CAI data indicate that conditions ranging from middle greenschist to subgreenschist facies were attained in the hanging wall of the Gold Ace fault. The metamorphic grade discordance across the Gold Ace fault represents at least 100°C of temperature difference, or ≈4 km difference in crustal levels, assuming a Cretaceous geothermal gradient of ≈28°C/km (discussed later).

## Significance of the Metamorphism

The pressure estimate obtained from geobarometry in the metamorphosed block (5.3±1.5 kb) indicates depths of 18.6±5.3 km. The rocks attained greater depth than the thickness of the sedimentary package, which is estimated to be ≈9 km based on 6.2 km from the Cambrian Wood Canyon Formation to the Mississippian Eleana Formation (Monsen and others, 1992) and adding several kilometers for possible Pennsylvanian and early Mesozoic units that are not found in the immediate area. Because substantial plutons to provide heat for the metamorphism are lacking, the metamorphism must have been related to tectonic burial by thrusting and folding. The correlation between temperature and depth across the thrust fault in the northeastern part of Bare Mountain, determined from the conodont color-alteration index data of Grow and others (1994), is consistent with this interpretation. The depth and temperature conditions for the metamorphism imply that the geothermal gradient at the time of metamorphism was 27°C/km (+12°, –6°).

In any setting where local heat sources, such as plutons, are absent, isotherms are likely to be subhorizontal isobaric planes. Lateral variations in grade observed at the surface, as at northwestern Bare Mountain, are indicative of postmetamorphism tilting. Because no significant local heat sources exist within the metamorphosed block at Bare Mountain, the garnet-staurolite isograd in the northwestern area probably represents a southeast-tilted isobaric surface. Limits can be placed on the amount of tilt. Within the metamorphosed block, biotite is stable in mica schists to the southernmost point, indicating that temperatures everywhere were greater than about 450°C. This compares to about 530°C attained in garnet-bearing mica schists from the northwest corner. The temperature drop southeastward across the metamorphosed block is therefore equal to or less than 80°C. Considering that the distance across which the temperature drop takes place is approximately 7 km, and assuming a geothermal gradient of 28°C/km (discussed previously), it follows that the tilt is no more than 25° to the southeast. Because of large uncertainties associated with the values in the calculation, the tilt angle carries meaning only insofar as to indicate a gentle tilt to the southeast.

**Table 4.** Minerals, modes, and activity assumptions for the calculation of garnet-in and chlorite-out isopleths in figure 5.

[Based on F0 mineral analysis data for sample 50d and garnet "F0 core 5-6"; — , pure end-member composition was assumed]

| Phase | Activity model | Analysis from table 2 | Initial mode (volume percent) |
|---|---|---|---|
| α-Quartz | Pure end member | — | 48 |
| Muscovite | Pure end member | — | 26 |
| Plagioclase | Na-Ca ideal molecular activity model | F0 | 13 |
| Biotite | Fe-Mg-Mn ideal mixing activity model | F0 Bio | 11 |
| Water | Pure end member | — | 0 |
| Chlorite | Fe-Mg-Mn ideal mixing activity model | F1/F0 | 2 |
| Garnet | Ca-Fe-Mg-Mn ideal mixing activity model | F0 core 5-6 | 0 |

**Table 5.** Changes in mode (ΔM) and composition (ΔX) between garnet-in and chlorite-out isopleths at 5 kilobars.

[Based on "F0" mineral analysis data for sample 50d and garnet "F0 core 5-6"; compositional variables are defined in tables 2*A*–*D*]

| Phase | Initial modes (Moles/100 $cm^3$ rock) | ΔM (moles) | Compositional variables | Initial values | ΔX |
|---|---|---|---|---|---|
| Quartz | 2.1157 | –0.0149 | | | |
| Muscovite | 0.1831 | –0.0005 | | | |
| Plagioclase | 0.1285 | –0.0020 | $X_{ab}$ | 0.7510 | 0.0120 |
| | | | $X_{an}$ | 0.2490 | –0.0120 |
| Biotite | 0.0718 | 0.0006 | $X_{phl}$ | 0.4860 | 0.0635 |
| | | | $X_{ann}$ | 0.5110 | –0.0605 |
| | | | $X_{Mn}$ | 0.0033 | –0.0030 |
| Water | 0.0000 | 0.0372 | | | |
| Chlorite | 0.0093 | –0.0093 | $X_{clin}$ | 0.5536 | 0.0598 |
| | | | $X_{daph}$ | 0.4439 | –0.0575 |
| | | | $X_{Mn}$ | 0.0025 | –0.0023 |
| Garnet | 0.0000 | 0.0148 | $X_{py}$ | 0.1322 | 0.0869 |
| | | | $X_{al}$ | 0.6166 | 0.0991 |
| | | | $X_{sp}$ | 0.1633 | –0.1479 |
| | | | $X_{gr}$ | 0.0880 | –0.0380 |

**Table 6.** Garnet-biotite and garnet-chlorite geothermometric determinations in rocks from northwestern Bare Mountain.

[Temperatures in degrees Celsius. Calculations were performed using garnet-biotite geothermometer of Hodges and Spear (1982) and garnet-chlorite geothermometer of Grambling (1990) with pressure of 5 kb. Analyses are listed in table 2; *, biotite analyses corrected for the effects of retrogradation and metasomatism (see table 2*B*)]

| Garnet | Biotite | | | | | | | | Chlorite | | |
|---|---|---|---|---|---|---|---|---|---|---|---|
| | F1Bio | F1 Bio* | F0 Bio | F0 Bio* | 26b | 26b* | 39b | 39b* | F1/F0 | 26b | 39b |
| F1 rim 1 | 698 | 547 | | | | | | | 581 | | |
| F1 rim 2 | 669 | 525 | | | | | | | 568 | | |
| F0 rim 3 | | | 699 | 550 | | | | | 584 | | |
| F0 rim 4 | | | 686 | 541 | | | | | 575 | | |
| F0 rim 5 | | | 676 | 533 | | | | | 571 | | |
| F0 rim 6 | | | 616 | 490 | | | | | 530 | | |
| 26b rim 1 | | | | | 697 | 548 | | | | 593 | |
| 26b rim 2 | | | | | 613 | 487 | | | | 541 | |
| 26b rim 3 | | | | | 709 | 560 | | | | 593 | |
| 26b rim 4 | | | | | 687 | 539 | | | | 588 | |
| 39b rim 3 | | | | | | | 762 | 528 | | | 566 |
| 39b rim 4 | | | | | | | 727 | 507 | | | 547 |

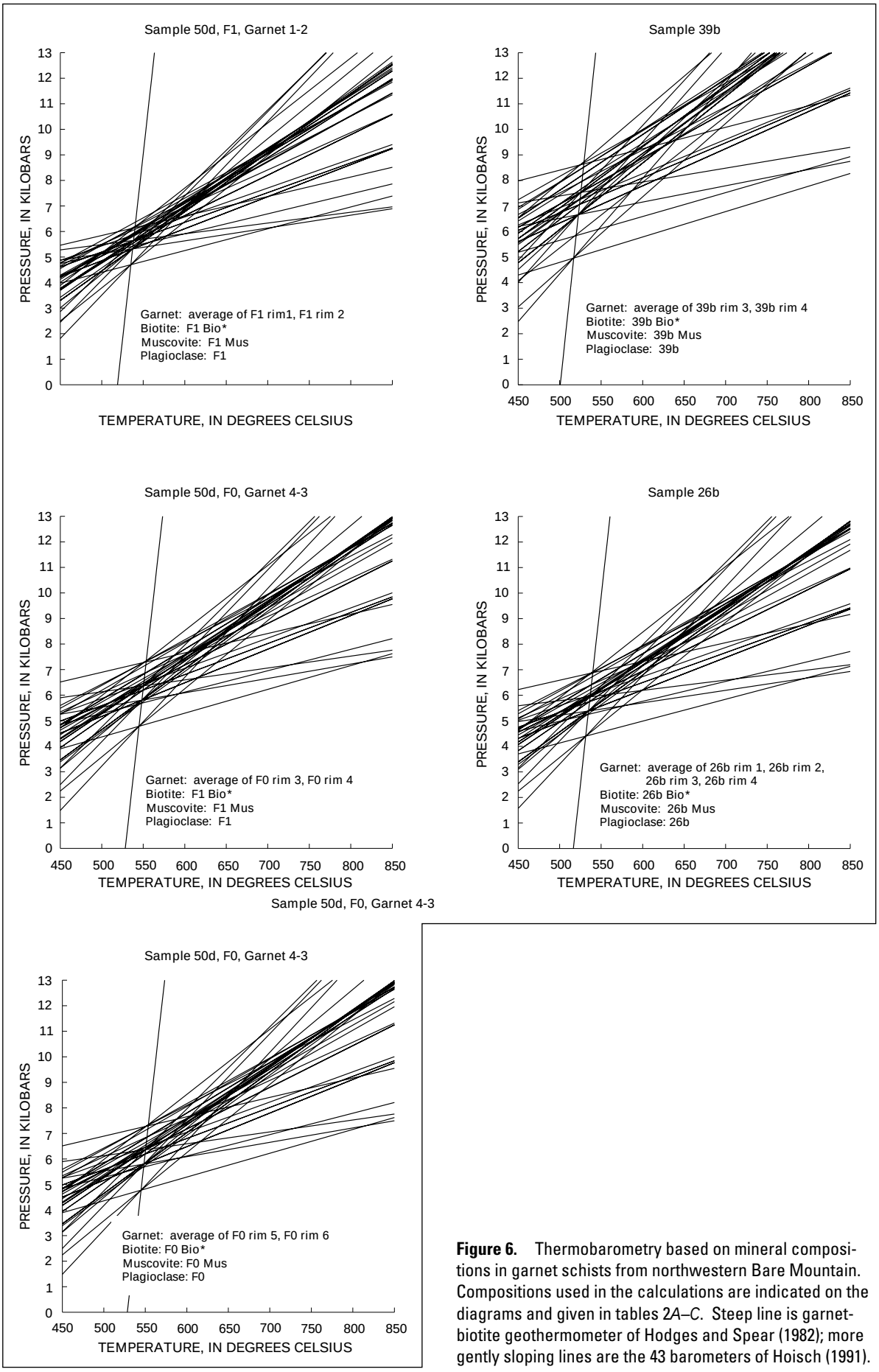


**Figure 6.** Thermobarometry based on mineral compositions in garnet schists from northwestern Bare Mountain. Compositions used in the calculations are indicated on the diagrams and given in tables 2*A*–*C*. Steep line is garnet-biotite geothermometer of Hodges and Spear (1982); more gently sloping lines are the 43 barometers of Hoisch (1991).

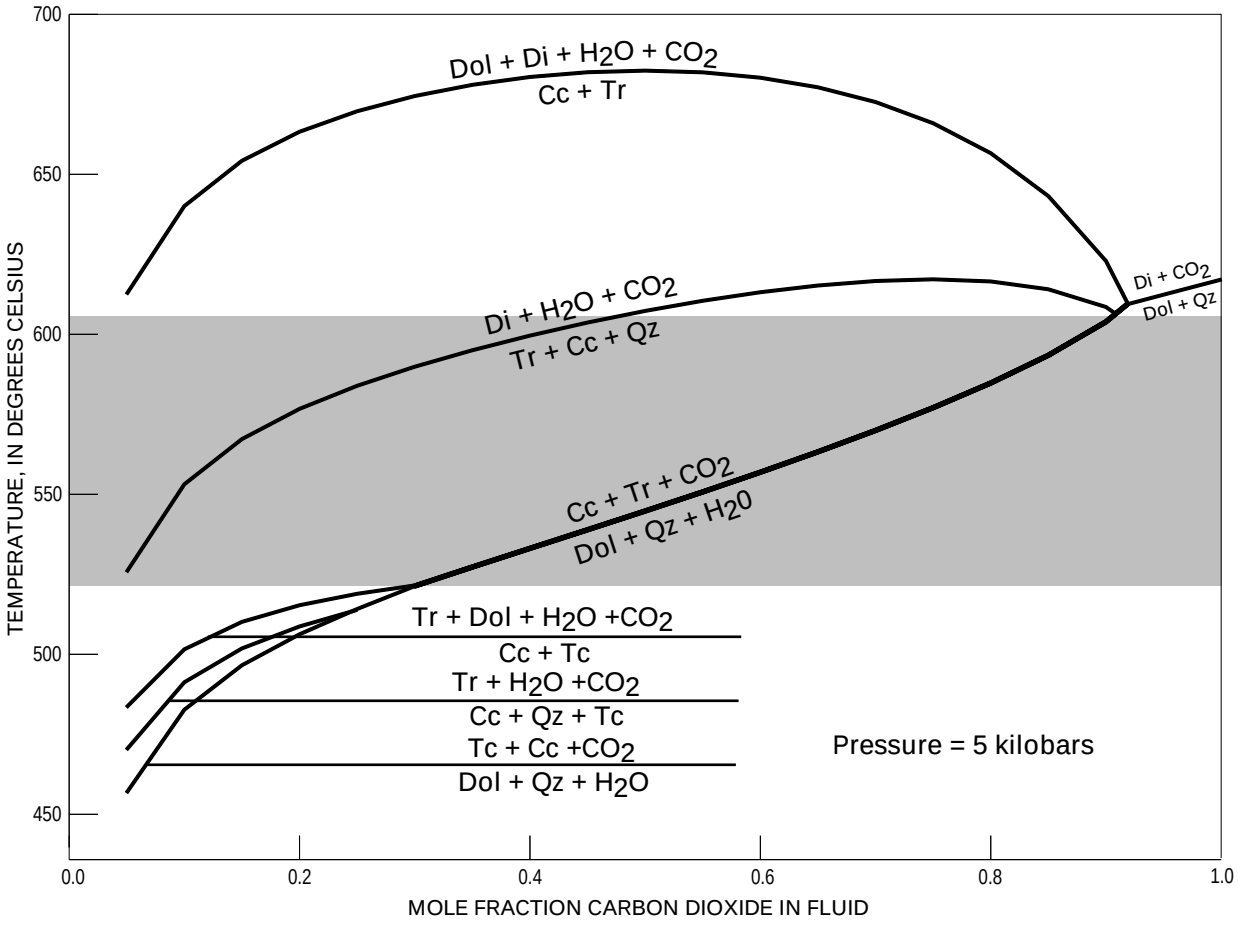


**Figure 7.** Selected reactions in the system MgO-CaO-$SiO_2$-$CO_2$-$H_2O$ at 5 kilobars. Shaded temperature interval is consistent with mineral assemblages observed in siliceous metadolomite from northwestern Bare Mountain (table 2*B*). Calculated using data and methods of Berman (1988a), mixed fluid ($H_2O$-$CO_2$) thermodynamic properties of Kerrick and Jacobs (1981), and calcite activity model of Skippen (1974) to account for the temperature-dependent solubility of Mg in calcite. Points on curves were calculated at intervals of $X(CO_2)$=0.05. Lines have not been adjusted to enhance convergence at invariant points. Cc, calcite; Di, diopside; Dol, dolomite; Qz, quartz; Tc, talc; Tr, tremolite.

As noted by Monsen (1979), the garnet-staurolite isograd cuts across stratigraphy, and the metamorphic grade changes within individual stratigraphic units. These characteristics suggest that the strata were moderately or steeply dipping during metamorphism and were subsequently rotated. At Bare Mountain, dipping strata at depth would be an expected consequence of thrust faulting prior to metamorphism, and subsequent tilting an expected consequence of detachment faulting.

Lineations and kinematic indicators in calc-mylonites along the Boundary Canyon fault in the northern Funeral Mountains indicate relatively west-northwestward slip of the upper plate (Hoisch and Simpson, 1993), which is consistent with the movement direction inferred from faulting in the upper plate at Bare Mountain and in the Bullfrog Hills (Maldonado, 1990; Monsen and others, 1992). The hanging wall of the Gold Ace fault narrows to the northwest beneath the higher level Fluorspar Canyon fault (fig. 2). Farther to the west, slivers of Paleozoic strata of subgreenschist facies grade are present beneath the Bullfrog detachment fault. Grow and others (1994) reported conodont color-alteration indexes from these slivers that are similar to data from subgreenschist-facies rocks in the hanging wall of the Gold Ace fault at Bare Mountain. The subgreenschist slivers may have originated at Bare Mountain by excision of the lower part of the upper plate as movement along the detachment fault progressed.

There are important differences between the metamorphosed block at Bare Mountain and the lower plates of the Boundary Canyon fault and the Bullfrog detachment fault. The lower-plate rocks in the northwest part of the Funeral Mountains and Bullfrog Hills are middle to upper amphibolite facies, whereas the metamorphosed block at Bare Mountain is upper greenschist to lower amphibolite facies. The lower plates of the Boundary Canyon fault and the Bullfrog detachment fault are strongly mylonitic whereas Bare Mountain is not. The lower plates of the Boundary Canyon fault and the Bullfrog detachment fault involve older strata that are about 5 km deeper in the section than those at Bare Mountain and are injected by dikes of Late Cretaceous muscovite granite whereas such dikes are sparse at Bare Mountain. These factors suggest that the detachment fault extended downward to the west-northwest at a

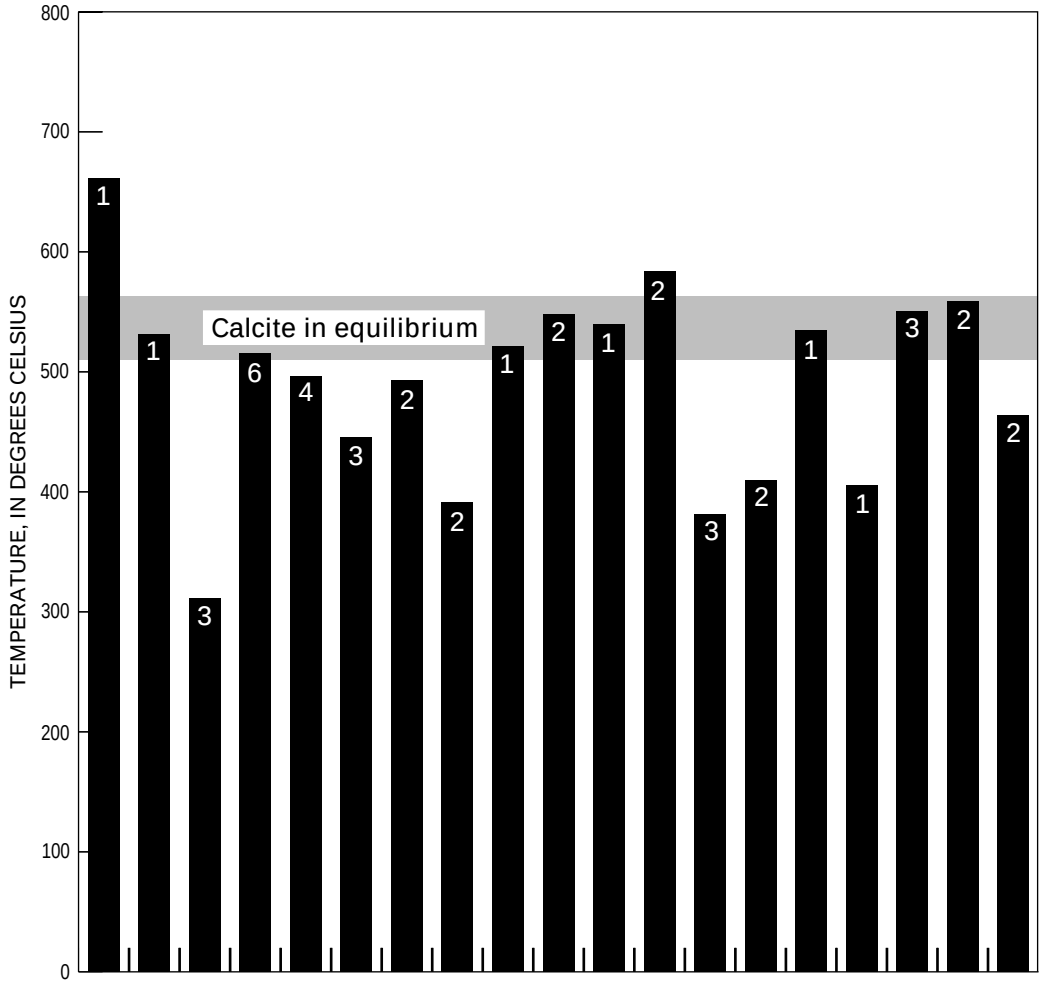


**Figure 8.** Calcite-dolomite geothermometry (Anovitz and Essene, 1987) of 19 calcite grains from sample 40 from northwestern Bare Mountain. Number at top of bar indicates number of analyses averaged for an individual grain. Shaded temperature interval (510°–560°C) indicates peak temperature attained in the rock (see text for explanation).

moderate angle to depths below the brittle-ductile transition where it was a shear zone. The lower plate at Bare Mountain was denuded from shallow crustal levels and the lower plate in the Funeral Mountains and Bullfrog Hills was denuded from deep crustal levels. This is consistent with the rolling hinge model of detachment faulting (for example, Hamilton, 1988a, 1988b; Wernicke and Axen, 1988), in which a normal fault that initiates at a moderate dip undergoes rotation to a subhorizontal orientation as fault movement progresses.

## Timing of Detachment Faulting

Based on the dating of upper-plate rocks and their relationships to faults, Weiss and others (1991) concluded that the Bullfrog detachment fault was active between 11 and 9 Ma. Fission-track ages from lower-plate rocks indicate rapid cooling at about the same time (Hoisch and others, 1997). Fission-track ages of zircon and apatite from lower-plate metamorphic rocks at Bare Mountain indicate rapid cooling from 12.6 to 11.1 Ma (Hoisch and others, 1997). Additional thermochronologic data reported in Hoisch and others (1997) were interpreted to indicate that the rapid cooling was preceded by slow cooling in both these areas. Similarly, fission-track ages of apatite, sphene, and zircon from lower-plate rocks in the northern Funeral Mountains indicate that rapid cooling took place from 11 to 6 Ma (Hoisch and Simpson, 1993; Holm and Dokka, 1991). The slow cooling was interpreted to be a result of about 9 km of unroofing by slow erosion of a topographic highland, and the subsequent rapid cooling was attributed to 9 km of rapid unroofing by tectonic denudation related to detachment faulting (Hoisch and others, 1997).

The earliest deformation related to crustal extension in the region may be reflected in the ductile quartz fabrics preserved in the lower plate in the northern Funeral Mountains and in the Bullfrog Hills. These fabrics are regarded as part of a northwest-dipping extensional shear zone active in the middle and lower crust (Hoisch and Simpson, 1993). The shear zone may represent an early stage in a continuum of deformation which, following unroofing and cooling of the lower plate, culminated with detachment faulting (Hoisch and Simpson, 1993). Applegate and others (1992), however, interpreted the fabrics to be Late Cretaceous in age and unrelated to the Miocene detachment fault.

## Conclusions

A fault-bounded block of lower amphibolite to upper greenschist facies metamorphic rocks is present in the northwest corner of Bare Mountain. The block is flanked on the north by a gently north dipping normal (detachment) fault, the Fluorspar Canyon fault, and on the east by a moderately east dipping normal fault, the Gold Ace fault. Calcite-dolomite geothermometry and mineral assemblages in garnet schist and siliceous metadolomite indicate peak temperatures of about 530°C. Thermobarometry applied to garnet schist yielded pressures of 5.3±1.5 kb, which equates to a depth of 18.6±5.3 km. To perform thermobarometric calculations, it was necessary to correct the biotite compositions for the effects of retrograde metasomatism, which caused Fe-enrichment. A gentle southeast tilt of the metamorphosed block is inferred from a gradual decrease in metamorphic grade to the southeast. About 3 km south of the northwest corner, an isograd delineates the southern limit of garnet and staurolite in the Wood Canyon Formation.

Thermochronologic data (Hoisch and others, 1997) indicate that of the 18 km of unroofing, about 9 km took place slowly from the Early Cretaceous peak of metamorphism to the onset of detachment faulting and might have resulted from surface erosion. About 9 km of rapid unroofing at 12.6 to 11.1 Ma followed the slow unroofing and was a consequence of tectonic denudation by detachment faulting.

In the hanging wall of the Gold Ace fault are fossiliferous shales in a thick Paleozoic sequence of mainly carbonate rocks. Conodont color-alteration indexes indicate conditions of middle greenschist to subgreenschist facies. The difference in metamorphic grade across the fault suggests a normal component of displacement of ≈4 km. The hanging wall of the Gold Ace fault narrows to the west beneath the Fluorspar Canyon fault. Farther to the west in the Bullfrog Hills, slivers of Paleozoic rocks are present along the Bullfrog detachment fault. These slivers may have been excised from the lower part of the upper plate as west-northwest movement of the upper plate along the detachment fault progressed.

## References Cited


Anovitz, L.M., and Essene, E.J., 1987, Phase relations in the system $CaCO_3$-$MgCO_3$-$FeCO_3$: Journal of Petrology, v. 28, p. 389–414.

Applegate, J.D.R., 1994, The unroofing history of the Funeral Mountains metamorphic core complex, California: Cambridge, Mass., Massachusetts Institute of Technology Ph. D. thesis, 241 p.

Applegate, J.D.R., Walker, J.D., and Hodges, K.V., 1992, Late Cretaceous extensional unroofing in the Funeral Mountains metamorphic core complex: Geology, v. 20, p. 519–522.

Berman, R.G., 1988a, Internally-consistent thermodynamic data for minerals in the system $Na_2O$-$K_2O$-CaO-MgO-FeO-$Fe_2O_3$-$Al_2O_3$-$SiO_2$-$TiO_2$-$H_2O$-$CO_2$: Journal of Petrology, v. 29, p. 445–522.

———1988b, A general method for thermobarometric calculations, with a revised garnet solution model and geologic applications: Geological Society of America Abstracts with Programs, v. 20, no. 7, p. A98.

Berman, R.G., and Brown, T.H., 1985, The heat capacity of minerals in the system $Na_2O$-$K_2O$-CaO-MgO-FeO-$Fe_2O_3$-$Al_2O_3$-$SiO_2$-$TiO_2$-$H_2O$-$CO_2$—Representation, estimation, and high temperature extrapolation: Contributions to Mineralogy and Petrology, v. 89, p. 168–183.

Bohlen, S.R., Wall, V.J., and Boettcher, A.L., 1983, Geobarometry in granulites, *in* Saxena, S.K., ed., Kinetics and equilibrium in mineral reactions: New York, Springer-Verlag, p. 141–171.

Bowman, J.R., and Essene, E.J., 1982, P-T-X($CO_2$) conditions of contact metamorphism in the Black Butte aureole, Elkhorn, Montana: American Journal of Science, v. 282, p. 311–340.

Carr, M.D., and S.A. Monsen, 1988, A field trip guide to the geology of the Bare Mountain, *in* Weide, D.L., and Faber, M.L., eds., This extended land—Geological journeys in the southern Basin and Range: Geological Society of America, Cordilleran Section, Field Trip Guidebook, Special Publication 2, University of Nevada Geoscience Department, Las Vegas, p. 50–57.

Cornwall, H.R., and Kleinhampl, F.J., 1961, Geology of the Bare Mountain quadrangle: U.S. Geological Survey Geologic Quadrangle Map GQ-157, scale 1:62,500.

DeWitt, E.J., Sutter, J.F., Wright, L.A., and Troxel, B.W., 1988, Ar-Ar chronology of Early Cretaceous regional metamorphism, Funeral Mountains, California—A case study of excess argon: Geological Society of America Abstracts with Programs, v. 20, no. 7, p. A16.

Essene, E.J., 1982, Geologic thermometry and barometry, *in* Ferry, J.M., ed., Characterization of metamorphism through mineral equilibria: Reviews in Mineralogy, v. 10, p. 153–206.

Florence, F.P., and Spear, F.S., 1993, Influences of reaction history and chemical diffusion on P-T calculations for staurolite schists from the Littleton Formation, northwestern New Hampshire: American Mineralogist, v. 78, p. 345–359.

Frizzell, V.A., Jr., and Shulters, Jacqueline, 1990, Geologic map of the Nevada Test Site, southern Nevada: U.S. Geological Survey Miscellaneous Investigations Map I-2046, scale 1:100,000.

Glen, J.M., and Ponce, D.A., 1991, Aeromagnetic maps of the Beatty quadrangle, Nevada-California: U.S. Geological Survey Open-File Report 91-105, scale 1:100,000.

Grambling, J.A., 1990, Internally-consistent geothermometry and $H_2O$ barometry in metamorphic rocks—The example garnet-chlorite-quartz: Contributions to Mineralogy and Petrology, v. 105, p. 617–628.

Grow, J.A., Barker, C.E., and Harris, A.G., 1994, Oil and gas exploration near Yucca Mountain, southern Nevada: Proceedings of the American Nuclear Society, International High Level Radioactive Waste Management Conference, Las Vegas, May 22–26, v. 3, p. 1298–1315.

Haar, Lester, Gallagher, J.S., and Kell, G.S., 1984, NBS/NRC steam tables— Thermodynamic and transport properties and computer programs for vapor and liquid states of water in SI units: Washington, D.C., Hemisphere Publishing Co., 320 p.

Hamilton, W.B., 1988a, Detachment faulting in the Death Valley region, California and Nevada, *in* Carr, M.D., and Yount, J.C., eds., Geologic and hydrologic investigations of a potential nuclear waste disposal site at Yucca Mountain, Nevada: U.S. Geological Survey Bulletin 1790, p. 51–85.

———1988b, Death Valley tectonics—Hingeline between active and inactivated parts of a rising and flattening master normal fault, *in* Gregory, J.L., and Baldwin, E.J., eds., Geology of the Death Valley region: South Coast Geological Society Field Trip Guidebook, Santa Ana, Calif., v. 16, p. 179–205.

Hodges, K.V., and Spear, F.S., 1982, Geothermometry, geobarometry, and the $Al_2SiO_5$ triple point at Mt. Moosilauke, New Hampshire: American Mineralogist, v. 67, p. 1118–1134.

Hodges, K.V., and Walker, J.D., 1990, Petrologic constraints on the unroofing history of the Funeral Mountains metamorphic core complex, California: Journal of Geophysical Research, v. 95, p. 8437–8445.

Hoisch, T.D., 1991, Equilibria within the mineral assemblage quartz+muscovite+biotite+garnet+plagioclase: Contributions to Mineralogy and Petrology, v. 108, p. 43–54.

Hoisch, T.D., Heizler, M.T., and Zartman, R.E., 1997, Timing of detachment faulting in the Bullfrog Hills and Bare Mountain area, southwest Nevada—Inferences from $^{40}Ar/^{39}Ar$, K-Ar, U-Pb, and fission track thermochronology: Journal of Geophysical Research, v. 102, p. 2815–2833.

Hoisch, T.D., and Simpson, Carol, 1993, Rise and tilt of metamorphic rocks in the lower plate of a detachment fault in the Funeral Mountains, Death Valley, California: Journal of Geophysical Research, v. 98, p. 6805–6827.

Holland, T.J.B., 1989, Dependence of entropy on volume for silicate and oxide minerals—A review and a predictive model: American Mineralogist, v. 74, p. 5–13.

Holm, D.K., and Dokka, R.K., 1991, Major late Miocene cooling of the middle crust associated with extensional orogenesis in the Funeral Mountains, California: Geophysical Research Letters, v. 18, p. 1775–1778.

———1993, Interpretation and tectonic implications of cooling histories—An example from the Black Mountains, Death Valley extended terrane, California: Earth and Planetary Science Letters, v. 116, p. 63–80.

Holm, D.K., Geissman, J.W., and Wernicke, Brian, 1993, Tilt and rotation of the footwall of a major normal fault system—Paleomagnetism of the Black Mountains, Death Valley extended terrane, California: Geological Society of America Bulletin, v. 105, p. 1373–1387.

Holm, D.K., Snow, J.H., and Lux, D.R., 1992, Thermal and barometric constraints on the intrusive and unroofing history of the Black Mountains—Implications for the timing, initial dip, and kinematics of detachment faulting in the Death Valley region, California: Tectonics, v. 11, p. 507–522.

Holm, D.K., and Wernicke, Brian, 1990, Black Mountains crustal section, Death Valley extended terrain, California: Geology, v. 18, p. 520–523.

Kerrick, D.M., and Jacobs, G.K., 1981, A modified Redlich-Kwong equation for $H_2O$, $CO_2$, and $H_2O$-$CO_2$ mixtures at elevated pressures and temperatures: American Journal of Science, v. 281, p. 735–767.

Maldonado, Florian, 1990, Geologic map of the northwest quarter of the Bullfrog 15-minute quadrangle, Nye County, Nevada: U.S. Geological Survey Miscellaneous Investigations Map I-1985, scale 1:24,000.

Maldonado, Florian, and Hausback, B.P., 1990, Geologic map of the northeast quarter of the Bullfrog 15-minute quadrangle, Nye County, Nevada: U.S. Geological Survey Miscellaneous Investigations Map I-2049.

Monsen, S.A., 1979, Structural evolution and metamorphic petrology of the Precambrian-Cambrian strata, northwest Bare Mountain, Nevada: Davis, Calif., University of California M.S. thesis, 66 p.

Monsen, S.A., Carr, M.D., Reheis, M.C., and Orkild, P.P., 1992, Geologic map of Bare Mountain, Nye County, Nevada: U.S. Geological Survey Miscellaneous Investigations Map I-2201, scale 1:24,000.

Newton, R.C., and Haselton, H.T., 1981, Thermodynamics of the garnet-plagioclase-$Al_2SiO_5$-quartz geobarometer, *in* Newton, R.C., Navrotsky, Alexandra, and Wood, B.J., eds., Thermodynamics of minerals and melts: New York, Springer-Verlag, p. 131–147.

Powell, Roger, and Holland, T.J.B., 1985, An internally consistent thermodynamic dataset with uncertainties and correlations—1, Methods and a worked example: Journal of Metamorphic Geology, v. 3, p. 327–342.

Rejebian, V.A., Harris, A.G., and Heubner, J.S., 1987, Conodont color and textural alteration—An index to regional metamorphism, contact metamorphism, and hydrothermal alteration: Geological Society of America Bulletin, v. 99, p. 471–479.

Skippen, G.B., 1974, An experimental model for low pressure metamorphism of siliceous dolomitic marble: American Journal of Science, v. 274, p. 487–509.

Spear, F.S., 1988, The Gibbs method and Duhem's theorem—The quantitative relationships among P, T, chemical potential, phase composition and reaction progress in igneous and metamorphic systems: Contributions to Mineralogy and Petrology, v. 99, p. 249–256.

———1989, Petrologic determination of metamorphic pressure-temperature-time paths, *in* Crawford, M.L., and Padovani, E., eds., Metamorphic pressure-temperature-time paths: American Geophysical Union, Short Course in Geology, v. 7, 55 p.

———1993, Metamorphic phase equilibria and pressure-temperature-time paths: Mineralogical Society of America Monograph, 799 p.

Spear, F.S., and Cheney, J.T., 1989, A petrogenetic grid for pelitic schists in the system $SiO_2$-$Al_2O_3$-FeO-MgO-$K_2O$-$H_2O$: Contributions to Mineralogy and Petrology, v. 101, p. 149–164.

Spear, F.S., and Florence, F.P., 1992, Thermobarometry in granulites—Pifalls and new approaches: Precambrian Research, v. 55, p. 209–241.

Spear, F.S., Peacock, S.M., Kohn, M.J., Florence, F.P., and Menard, T., 1991, Computer programs for petrologic P-T-t calculations: American Mineralogist, v. 76, p. 2009–2012.

Tracy, R.J., 1982, Compositional zoning and inclusions in metamorphic minerals, *in* Ferry, J.M., ed., Characterization of metamorphism through mineral equilibria: Reviews in Mineralogy, v. 10, p. 355–397.

Weiss, S.L., McKee, E.H., Noble, D.C., Conners, K.A., and Jackson, M.R., 1991, Multiple episodes of Au-Ag mineralization in the Bullfrog Hills, SW Nevada, and their relation to coeval extension and volcanism: Geological Society of America Abstracts with Programs, v. 23, p. A246.

Wernicke, B., and Axen, G.J., 1988, On the role of isostacy in the evolution of normal fault systems: Geology, v. 16, p. 848–851.

Wright, L.A., and Troxel, B.W., 1993, Geologic map of the central and northern Funeral Mountains and adjacent areas, Death Valley region, southern California: U.S. Geological Survey Miscellaneous Investigations Map I-2305, scale 1:48,000.